Hindawi
Structural Control and Health Monitoring
Volume 2023, Article ID 6696148, 26 pages
https://doi.org/10.1155/2023/6696148

Research Article

Vibration Control of the Steel-Concrete Composite Box Girder Bridge with Slip and Shear-Lag Effects by MTMDs under the Train-Bridge Interaction

Qing-Chen Tang and Li Zhu

Beijing Jiaotong University, Beijing, China

Correspondence should be addressed to Li Zhu; zhuli@bjtu.edu.cn

Received 7 March 2023; Revised 19 April 2023; Accepted 2 June 2023; Published 27 June 2023

Academic Editor: Andrea Del Grosso

Steel-concrete composite girder bridges, in essence, are thin-walled structures, the dynamic responses of which will be greater than those of a typical Euler–Bernoulli beam under the train-bridge interaction because of the shear lag and interface slip. Thus, in this study, the dynamic analysis model of a train-composite box girder bridge-multiple tuned mass damper (MTMD) coupling system is proposed, with the derived dynamic equations of this time-varying system. Meanwhile, the program is compiled using the Newmark-β method for the solution, combined with the optimization toolbox to solve the complex optimization design problems of MTMDs involved. Finally, factors affecting the vibration-damping effect are studied, such as the mass ratio of MTMDs, the number of trains, and the slip and shear lag of the composite box girder bridge.

1. Introduction

Train-bridge coupling vibration is a strongly coupled time-varying parameter excitation problem, and many researchers worldwide have studied the mechanism of this coupled vibration [1–13]. However, when the spans of railway bridges become larger, the train's higher speed will cause excessive vibrations of them, posing a potential threat to its traffic and structural safety and comfort of passengers.

In addition, the steel-concrete composite box girder bridge is one of the thin-walled structures with relatively low stiffness. Thus, its special material and section properties also determine its special mechanical behaviors, i.e., shear lag due to a large width-span ratio [14–16], and interface slip caused by the fatigue deformation of shear studs between the concrete slab and the steel beam [17–19], as illustrated in Figure 1. To a certain extent, its dynamic responses under the train-bridge interaction will be greater than those of a typical Euler–Bernoulli beam because of these effects above [20, 21], and more importantly, cannot be ignored. Therefore, more reasonable and reliable steps must be taken to control the vibration of the composite girder bridge.

So, to achieve this, a simple and economical way, at first, was to install damping devices on the main structure, such as a tuned mass damper (TMD). In the past, Kwon et al. [22], Chen and Huang [23], Shi and Cai [24], Moghaddas et al. [25], Krenk and Høgsberg [26], Chun et al. [27], and Lievens et al. [28] have conducted intensive research on the classical TMD model and its mechanisms, which are relatively mature now. In fact, the TMD is realized by tuning its frequency at or near the corresponding one of a structure (generally the first-order natural frequency) to control its vibration. Obviously, it is a must to determine the frequency of a bridge accurately during the design stage of the TMD since it is sensitive to the frequency. However, in many engineering cases, due to errors of estimation during construction and the time-varying effect of a coupling system, the TMD may have a pronounced detuning effect, which greatly reduces the vibration-damping effect, and stability and reliability itself are not that strong.

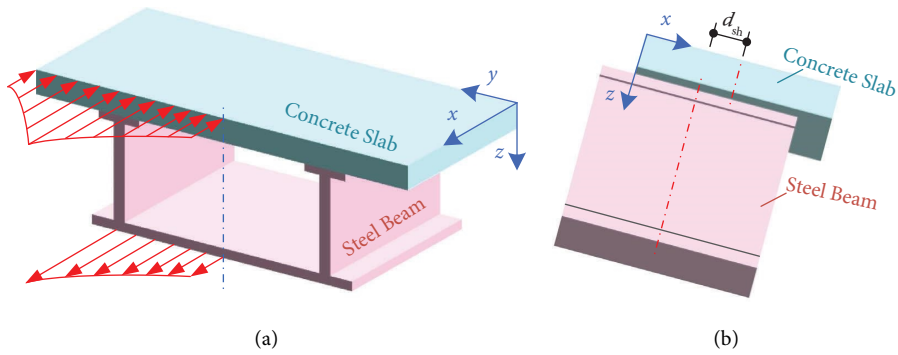

(a) (b)

Figure 1: Shear-lag and interface slip effects in the composite girder bridge: (a) shear lag; (b) interface slip.

On the contrary, an MTMD system composed of multiple smaller TMDs can be configured to effectively avoid these problems above because it has a larger bandwidth and aims at more excitation's frequencies than a TMD, not only dispersing its mass and volume but also possessing robustness to suppress the vibration better. Therefore, installing MTMDs on the bridge can validly reduce the resonant responses corresponding to the structure's mode [29, 30]. Yau and Yang [31, 32] developed a broadband MTMD system to control the vibration of continuous truss bridges under moving loads excited by trains. Lin et al. [29] found that once axle loads of trains are evenly distributed, MTMDs are more effective and reliable than an individual TMD to suppress the resonant responses of the bridge. Li et al. [33] discussed the TMD's dominant factors in an MTMD system and eventually obtained the optimum parameters of MTMDs in controlling the resonant responses of railway simply supported beam bridges induced by high-speed train loads. Luu et al. [34] were devoted to the optimization for high-speed railway bridges to control its multiresonant peaks by an MTMD system. Miguel et al. [35] studied the novel robust design optimization of MTMDs with the principle of maximum entropy and the firefly algorithm, successfully employing it into vehicle-bridge coupled random excitations. Kahya and Araz [36] presented a series of multiple tuned mass dampers (SMTMDs) aimed at high-speed railway continuous bridges and found that the SMTMD system is more capable of controlling the vibration than a typical TMD.

According to the studies mentioned above, the current focus of vibration control is mainly on concrete or steel bridges under train-bridge interactions, and the analysis model is relatively simple. Nevertheless, now, there are few steel-concrete composite girder bridges whose slip and shear-lag effects have not been considered, resulting in an inaccurate analysis of dynamic responses and thus the vibration-damping effect. Given the lack of available methods for vibration control aimed at the steel-concrete composite girder bridges under train-bridge self-excitations, its mechanisms need to be further studied. However, the composite girder bridge-train-MTMD system is a complex time-varying and coupled system, which renders it more difficult to optimize the parameters, and little else does so.

Hence, considering slip and shear-lag effects, in this study, the dynamic analysis model of a train-composite box girder bridge-MTMD coupling and time-varying system is proposed. Then, the matrices about the composite box girder bridge are derived to obtain the dynamic equations of this system. Meanwhile, the solution program is developed by employing the Newmark-β method, combined with the optimization toolbox to solve the problem of this complex optimization design problems with MTMDs involved, providing a novel approach for the optimization of the coupled time-varying system. Finally, the optimization method is employed in the numerical simulation to explore the factors affecting the MTMDs' vibration-damping effect based on train-bridge interactions, such as the mass ratio of MTMDs, the number of trains, and the slip and shear lag of the composite girder bridge.

2. Dynamic Analysis Model of a Train-Composite Box Girder Bridge Coupling System with Special Mechanical Behaviors

2.1. Dynamic Analysis Model of the Composite Box Girder Bridge. According to the research by Gara et al. [37], the steel-concrete composite girder bridge is located in the Cartesian coordinate system (within three directions), and its geometric parameters are shown in Figure 2.

In this coordinate system, the position vector of any point within the bridge can be demonstrated as

$$\mathbf{r}(x, y, z) = x\mathbf{ii} + y\mathbf{jj} + z\mathbf{kk}, \quad \forall (x, y) \in \{\overline{A}_c \cup \overline{A}_s\}, z \in [0, L], \tag{1}$$

where **ii**, **jj**, and **kk** are the unit vectors along three directions in Figure 2, respectively, $\overline{A}_c$ and $\overline{A}_s$ are the areas enveloped by the concrete slab and the steel beam, and L is the bridge's span.

To consider the shear-lag effect (see Figure 3), the shear warping intensity functions f_c and f_s and shear warping shape functions $\psi_c(y), \psi_s(y)$ are introduced, respectively, according to equations (2) and (3):

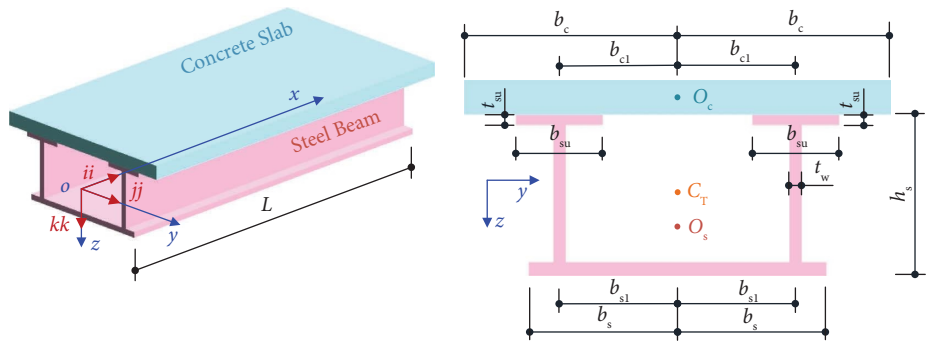

(a) (b)

FIGURE 2: The coordinate system and geometric parameters of the bridge: (a) Cartesian coordinate system; (b) cross section of the bridge.

$$\psi(x)\begin{cases} 1-\dfrac{x^2}{b_{s1}{}^2}, & |x| \le b_{s1} \cap (x \in \text{bottom flange}), \\ 0, & |x| > b_{s1} \cap (x \in \text{bottom flange}), \\ 0, & x \in \text{top flange}, \end{cases} \tag{2}$$

$$\psi(x)\begin{cases} 1-\dfrac{x^2}{b_{s1}{}^2}, & |x| \le b_{s1} \cap (x \in \text{bottom flange}), \\ 0, & |x| > b_{s1} \cap (x \in \text{bottom flange}), \\ 0, & x \in \text{top flange}. \end{cases} \tag{3}$$

Thus, combined with Figure 4, the translational displacement of any point in the composite girder bridge along three directions are

$$\begin{cases} u(x,y,z) = u_0(x) - \phi(x)\left(z - z_{C_T}\right), \\ v(x,y,z) = v_0(x) + \phi(x)\left(y - y_{C_T}\right), \\ w_m(x,y,z) = w_{m0}(x) - u_0'(x)(y - y_m) - v_0'(x)(z - z_m) + f_m(x)\psi_m(y), \end{cases} \tag{4}$$

where $m = c, s$ (referring to concrete and steel), u_0 and v_0 are the displacement of the composite box girder bridge along O-y and O-z directions, respectively, y_{C_T} and z_{C_T} are positions of the torsion center in the transformed section of the bridge along O-y and O-z directions, respectively, y_c, y_s are positions of centroids along the O-y direction, respectively, z_c and z_s along the O-z direction, w_{c0} and w_{s0} are displacements of centroids along the O-x direction, and ϕ is the angle of the bridge's free torsion (subscript $_c$ refers to the concrete slab and $_s$ to the steel beam).

Since there is no shear lag at the web of the steel beam, the interface slip displacement Δ_{sh} can be simplified as

$$\Delta_{sh}(x,y,z) = w_{s0}(x) - w_{c0}(x) + v_0'(x)h_o, \tag{5}$$

where h_o is the distance between centroids the concrete slab and the steel beam along the O-z direction.

On top of that, concrete and steel are always linearly elastic. As the shear studs are evenly arranged, its shear connection stiffness ρ_{sh} is constant along the O-x direction. Hence, its bond-slip force q_{sh} (x, y, z) is

$$q_{sh} = \rho_{sh}\Delta_{sh.} \tag{6}$$

According to the principle of virtual work, the virtual work equation is

$$\int_V \boldsymbol{\sigma} \cdot \nabla(\delta \mathbf{d}_b) = \int_V \mathbf{f}_b \cdot \delta \mathbf{d}_b + \int_{\partial V} \mathbf{f}_s \cdot \delta \mathbf{d}_b, \quad \forall(\delta \mathbf{d}_b) \neq 0, \tag{7}$$

where $\boldsymbol{\sigma}$ is the stress tensor, ∇ is the gradient operator, $\mathbf{f}_b$ and $\mathbf{f}_s$ are the body forces and surface forces, and V and ∂V represent its volume and surface area, respectively. $\delta \mathbf{d}_b$ represents the variation of the generalized displacements $\mathbf{d}_b$, which is

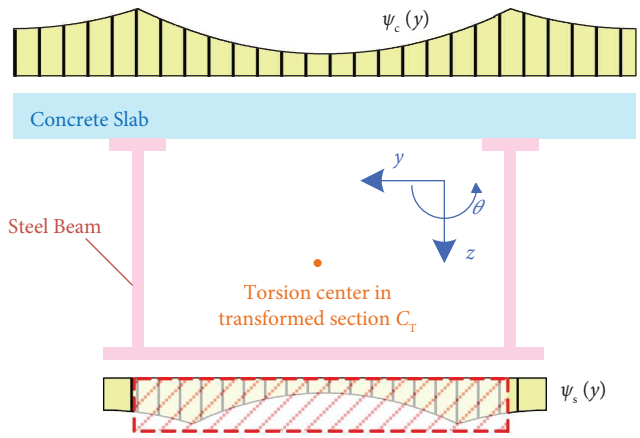

Figure 3: Shear-lag effect of the steel beam and concrete slab.

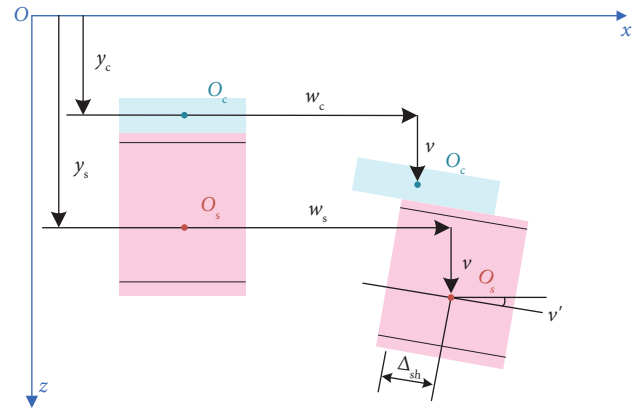

Figure 4: Displacements of the bridge.

$$\mathbf{d}_b^T(x) = [\, w_{c0}(x) \;\; w_{s0}(x) \;\; v_0(x) \;\; u_0(x) \;\; \phi(x) \;\; f_c(x) \;\; f_s(x) \,]. \tag{8}$$

Then, taking advantage of the finite element method and research by Zhu et al. [38] to solve equation (7), the girder bridge is discretized evenly into 3D finite beam elements (as shown in Figure 5), with two nodes and 18 degrees of freedom (DOFs) including its slip and shear-lag effects, each with 9 DOFs: $w_{cm}, w_{sm}, \phi_m, u_m, \varphi_m, v_m, \theta_m, f_{cm}$, and f_{sm}, where φ_m and θ_m are rotations around the O-y and O-z axes, respectively; subscripts i and j represent two nodes of the beam element, respectively.

Finally, the stiffness matrix $\mathbf{K}_{bb}$ and mass matrix $\mathbf{M}_{bb}$ can be obtained, respectively. Then, its damping matrix $\mathbf{C}_{bb}$ is derived from Rayleigh viscous damping theory (the derivations and expressions of all matrices and nonzero elements in research by Zhu et al. [38]).

2.2. Dynamic Analysis Model of a Train-Composite Box Girder Bridge Coupling System. The dynamic analysis model of a fine train-composite box girder bridge coupling system was adopted, as illustrated in Figure 6. As mentioned above, the composite box girder bridge model referred to Section 2.1 and the train were simulated according to a classical 27-DOF vehicle rigid body, including one car body (5 DOFs), two bogies (5 DOFs each), and four wheel sets (3 DOFs each); the symbolic representations of all geometric and characteristic parameters were consistent with the research by Zhu et al. [38]. Therefore, the dynamic equilibrium equations of this coupling system are

$$\begin{bmatrix} \mathbf{M}_{vv} & \mathbf{0} \\ \mathbf{0} & \mathbf{M}_{bb} \end{bmatrix} \begin{bmatrix} \ddot{\mathbf{q}}_v \\ \ddot{\mathbf{q}}_b \end{bmatrix} + \begin{bmatrix} \mathbf{C}_{vv} & \mathbf{0} \\ \mathbf{0} & \mathbf{C}_{bb} \end{bmatrix} \begin{bmatrix} \dot{\mathbf{q}}_v \\ \dot{\mathbf{q}}_b \end{bmatrix} + \begin{bmatrix} \mathbf{K}_{vv} & \mathbf{0} \\ \mathbf{0} & \mathbf{K}_{bb} \end{bmatrix} \begin{bmatrix} \mathbf{q}_v \\ \mathbf{q}_b \end{bmatrix} = \begin{bmatrix} \mathbf{F}_v \\ \mathbf{F}_b \end{bmatrix}, \tag{9}$$

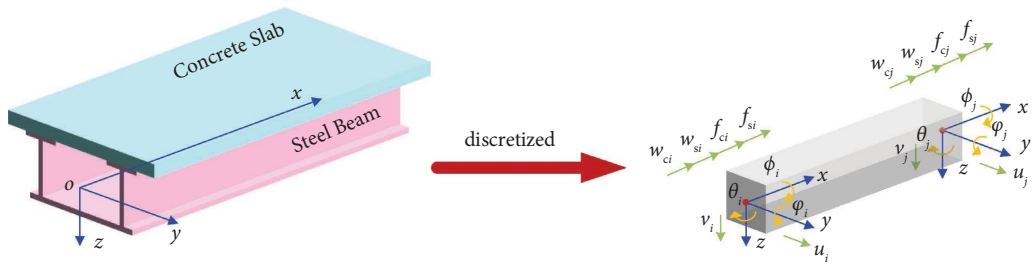

Figure 5: Finite beam element and the composite box girder bridge.

where $\mathbf{M}_{vv}$ and $\mathbf{K}_{vv}$ are matrices about the train's mass and stiffness in the global coordinate system, respectively, then, the damping matrix $\mathbf{C}_{vv}$ is Rayleigh viscous damping matrix, and $\mathbf{q}_v$ and $\mathbf{q}_b$ are displacement vectors of the train and the bridge, respectively. The dots on their top denote the derivative with respect to time. $\mathbf{F}_v$ and $\mathbf{F}_b$ are load vectors of each wheel set and the bridge in the global coordinate system, respectively.

We move some components of the load vector in equation (9), so that all elements about dynamic responses to be solved are on the left of equation (9), leaving the track irregularities on the right, and then, equation (9) owns the following form:

$$\begin{bmatrix} \mathbf{M}_{vv}^t & \mathbf{M}_{vb}^t \\ \mathbf{M}_{bv}^t & \mathbf{M}_{bb}^t \end{bmatrix} \begin{bmatrix} \ddot{q}_v^t \\ \ddot{q}_b^t \end{bmatrix} + \begin{bmatrix} \mathbf{C}_{vv}^t & \mathbf{C}_{vb}^t \\ \mathbf{C}_{bv}^t & \mathbf{C}_{bb}^t \end{bmatrix} \begin{bmatrix} \dot{\mathbf{q}}_v^t \\ \dot{\mathbf{q}}_b^t \end{bmatrix} + \begin{bmatrix} \mathbf{K}_{vv}^t & \mathbf{K}_{vb}^t \\ \mathbf{K}_{bv}^t & \mathbf{K}_{bb}^t \end{bmatrix} \begin{bmatrix} \mathbf{q}_v^t \\ \mathbf{q}_b^t \end{bmatrix} = \begin{bmatrix} \mathbf{F}_v^t \\ \mathbf{F}_b^t \end{bmatrix}, \tag{10}$$

where the superscript ^{t} indicates that nonzero elements within the matrix change as time goes. The results of its submatrix can be found in the study by Zhu et al. [38].

2.3. Consideration of the Rolling Contact. To better simulate the actual engineering situation, consider the coupling characteristics, and obtain exact responses of the system as trains pass over the composite girder bridge at a high speed, a more accurate wheel-rail rolling contact was introduced. Specifically, there is no relative displacement between the wheel set and the track both in the floating and rolling directions. However, in the yawing direction, based on Kalker elastic accurate creep theory [39], under the train coordinate system, the relationship between the wheel's lateral relative speed to the rail and the creep force F_{cy} (shown in Figure 7) was assumed to be approximately linear and expressed as

$$F_{cy} = -f_{cy}\xi_{cy} = -\frac{f_{cy}}{V}\left[\dot{u}_{vwijk} - \dot{u}_b\left(x_{vwijk}\right)\right], \tag{11}$$

where F_{cy} is the creep force in the y direction (yawing direction) under the train coordinate system, f_{cy} is the creep coefficient in the y direction, ξ_{cy} is the creepage, V is the train's operation speed, $\dot{u}_{vwijk}$ is the speed at the kth wheel set of the jth bogie in the ith car body, and $\dot{u}_b(x_{vwijk})$ is the bridge speed of the bridge corresponding to the kth wheel set of the jth bogie in the ith car body.

Therefore, the independent DOFs of the wheel set are only u_{vw} (yawing direction); v_{vw} (floating direction) and θ_{vw} (rolling direction) can be determined by the displacement of the bridge. In other words, the train model has 19 independent DOFs.

2.4. Validity of the Dynamic Analysis Model. Since this dynamic analysis model has been verified by an actual case in the research by Zhu et al. [38], where the Italia ETR 500Y train ($V = 288$ km/h) passed over a steel-concrete composite box viaduct ($7 \times 46 = 322$ m), the dynamic responses in time history agreed with the measured data, proving that the model was close to the real situation with validity.

Despite dealing with a more accurate wheel-rail rolling contact, this study only considered the transverse creep force in the direction, which made little difference in the vertical responses of the bridge. So the proposed model can still be effectively applicable to the following research.

3. Dynamic Analysis Model of a Train-Composite Box Girder Bridge-MTMD Coupling System with Special Mechanical Behaviors

3.1. MTMD System. Figure 8 illustrates an individual TMD device in the MTMD system installed on the composite box girder bridge. Dynamic equations of its vertical vibration can be given as

$$m_{ti}\ddot{v}_{ti} + c_{ti}\left(\dot{v}_{ti} - \dot{v}_{bl}\right) + k_{ti}\left(v_{ti} - v_{bl}\right) = 0 \quad (i = 1, 2, 3, \ldots, n), \tag{12}$$

where m_{ti}, c_{ti}, and k_{ti} are the mass, damping coefficient, and stiffness of an individual TMD, respectively, v_{ti} is the absolute vertical displacement of a TMD, and v_{bl} is absolute

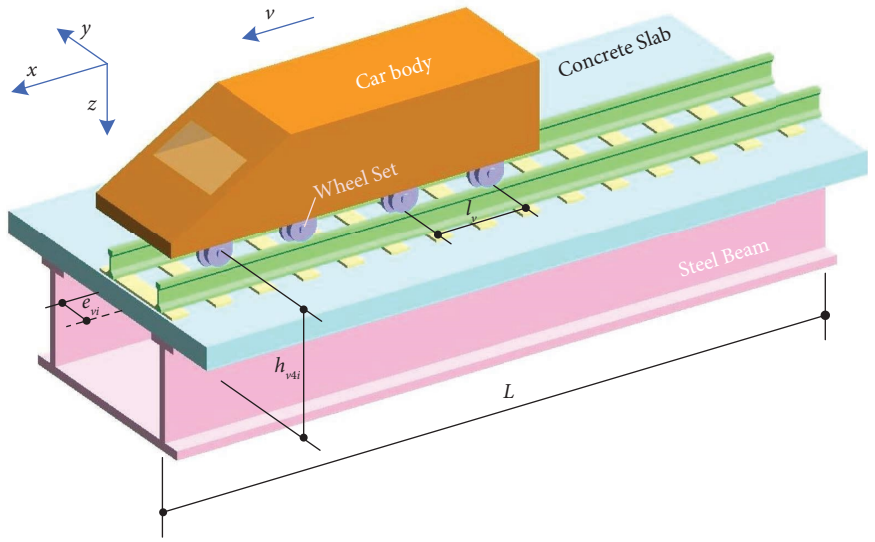

Figure 6: 3D train-composite box girder bridge-coupling system.

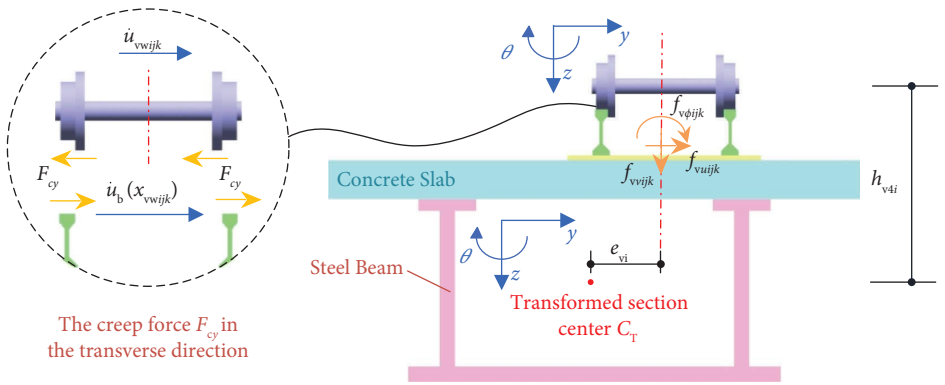

Figure 7: Concentrated loads of the wheels acting on the bridge.

vertical displacement of the lth beam element within the bridge where the TMD is installed.

After installing MTMDs on the composite box girder bridge ($x = x_{bl}$) exactly for vibration control, its dynamic equation for the vertical vibration can be

$$m_{bl}\ddot{v}_{bl} + c_{bl}\dot{v}_{bl} + k_{bl}v_{bl} = F_{bl} + F_T, \tag{13}$$

where m_{bl}, c_{bl}, k_{bl} are the consistent mass, damping coefficient, and stiffness of the lth beam element corresponding to where MTMDs are attached, respectively, F_{bl} is the lth beam element's node load vector exerted by wheel sets because of track irregularities, and F_T is the vector about the inertial force of MTMDs applied to the beam element, which can be expressed as

$$F_T = -\delta(x - x_{bl})\sum_{i=1}^{n} m_{ti}\ddot{v}_{ti} = \delta(x - x_{bl})\sum_{i=1}^{n}\left[c_{ti}(\dot{v}_{ti} - \dot{v}_{bl}) + k_{ti}(v_{ti} - v_{bl})\right], \tag{14}$$

where $\delta(-)$ is the Dirac function given as follows:

$$\delta(x - x_{bl}) = \begin{cases} 1, & (x = x_{bl}), \\ 0, & (x \neq x_{bl}). \end{cases} \tag{15}$$

Substituting equations (15) and (14) into equation (13), it can be simplified as

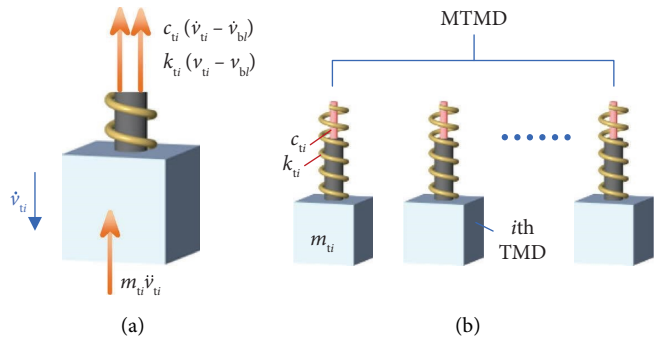

Figure 8: MTMD system and a TMD: (a) forces acting on a TMD; (b) MTMD system.

$$m_{bl}\ddot{v}_{bl} + \left(c_{bl} + \sum_{i=1}^{n} c_{ti}\right)\dot{v}_{bl} + \left(k_{bl} + \sum_{i=1}^{n} k_{ti}\right)v_{bl} = F_{bl} + \sum_{i=1}^{n}\left(c_{ti}\dot{v}_{ti} + k_{ti}v_{ti}\right). \tag{16}$$

3.2. A Fine Train-Composite Box Girder Bridge-MTMD Coupling System with Special Mechanical Behaviors. If a high-speed train operates at a uniform speed V on a composite girder bridge, any position within which the displacement of the track contacted by every wheel set is the superposition of displacements corresponding to bridge and track irregularities. In addition, MTMDs are hung inside to mitigate the bridge's vibration (see Figure 9). In this way, the dynamic equilibrium equation is

$$\begin{bmatrix} \mathbf{M}_{vv} & \mathbf{0} & \mathbf{0} \\ \mathbf{0} & \mathbf{M}_{bb} & \mathbf{0} \\ \mathbf{0} & \mathbf{0} & \mathbf{M}_{tt} \end{bmatrix}\begin{bmatrix} \ddot{\mathbf{q}}_v \\ \ddot{\mathbf{q}}_b \\ \ddot{\mathbf{q}}_t \end{bmatrix} + \begin{bmatrix} \mathbf{C}_{vv} & \mathbf{0} & \mathbf{0} \\ \mathbf{0} & \mathbf{C}_{bb} & \mathbf{C}_{bt} \\ \mathbf{0} & \mathbf{C}_{tb} & \mathbf{C}_{tt} \end{bmatrix}\begin{bmatrix} \dot{\mathbf{q}}_v \\ \dot{\mathbf{q}}_b \\ \dot{\mathbf{q}}_t \end{bmatrix} + \begin{bmatrix} \mathbf{K}_{vv} & \mathbf{0} & \mathbf{0} \\ \mathbf{0} & \mathbf{K}_{bb} & \mathbf{K}_{bt} \\ \mathbf{0} & \mathbf{K}_{tb} & \mathbf{K}_{tt} \end{bmatrix}\begin{bmatrix} \mathbf{q}_v \\ \mathbf{q}_b \\ \mathbf{q}_t \end{bmatrix} = \begin{bmatrix} \mathbf{F}_v \\ \mathbf{F}_b + \mathbf{F}_t \\ \mathbf{0} \end{bmatrix}, \tag{17}$$

where $\mathbf{F}_t$ is the column vector about inertia forces of MTMDs applied to the corresponding beam elements.

We move some components of the load vector in equation (17), so that all elements about dynamic responses to be solved are on the left, leaving the known track irregularities on the right. In addition, equation (17) has another following form:

$$\begin{bmatrix} \mathbf{M}^t_{vv} & \mathbf{M}^t_{vb} & \mathbf{0} \\ \mathbf{M}^t_{bv} & \mathbf{M}^t_{bb} & \mathbf{0} \\ \mathbf{0} & \mathbf{0} & \mathbf{M}_{tt} \end{bmatrix}\begin{bmatrix} \ddot{\mathbf{q}}^t_v \\ \ddot{\mathbf{q}}^t_b \\ \ddot{\mathbf{q}}_t \end{bmatrix} + \begin{bmatrix} \mathbf{C}^t_{vv} & \mathbf{C}^t_{vb} & \mathbf{0} \\ \mathbf{C}^t_{bv} & \mathbf{C}^t_{bb} & \mathbf{C}_{bt} \\ \mathbf{0} & \mathbf{C}_{tb} & \mathbf{C}_{tt} \end{bmatrix}\begin{bmatrix} \dot{\mathbf{q}}^t_v \\ \dot{\mathbf{q}}^t_b \\ \dot{\mathbf{q}}_t \end{bmatrix} + \begin{bmatrix} \mathbf{K}^t_{vv} & \mathbf{K}^t_{vb} & \mathbf{0} \\ \mathbf{K}^t_{bv} & \mathbf{K}^t_{bb} & \mathbf{K}_{bt} \\ \mathbf{0} & \mathbf{K}_{tb} & \mathbf{K}_{tt} \end{bmatrix}\begin{bmatrix} \mathbf{q}^t_v \\ \mathbf{q}^t_b \\ \mathbf{q}_t \end{bmatrix} = \begin{bmatrix} \mathbf{F}^t_v \\ \mathbf{F}^t_b \\ \mathbf{0} \end{bmatrix}, \tag{18}$$

where $\mathbf{q}_t$ is the displacement vector of MTMDs.

From equation (18) above, not only are some elements of the composite box girder bridge coupled with those of trains but also coupled with those of MTMDs. Meanwhile, the existing train components and bridge components themselves will be updated with the passage of time. Therefore, it has proved as a time-varying and coupled system.

To solve the second-order complex differential equations above, the Newmark-β method can be used in the iterative process. The elements of the stiffness submatrix $\mathbf{K}_{tt}$, mass submatrix $\mathbf{M}_{tt}$, and damping submatrix $\mathbf{C}_{tt}$ in the MTMD system and the nonzero MTMD-composite girder bridge coupling elements are elaborated in Appendix.

4. Vibration Control for Bridge and Optimum MTMD Design

4.1. The Numerical Example with Related Details. To investigate systematically the influence of the MTMD's mass ratio, the train's number, and the composite girder bridge's interface slip and shear lag on vibration control, according to the study by Tang et al. [41], an example is taken that a series of German ICE3 trains (all the parameters listed in Table 1) run over a mono-track railway simply supported by a steel-concrete composite box girder bridge ($L = 40$ m), as shown in Figure 10. The track irregularities refer to the sixth-grade power spectral density (PSD) according to the U.S. railway standard.

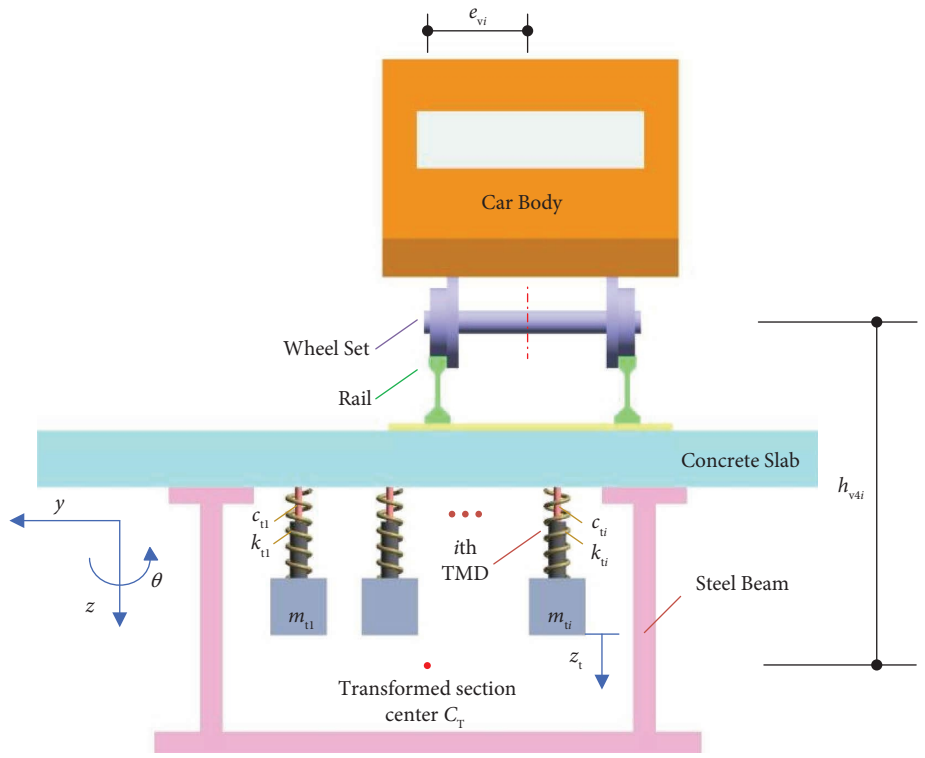

Figure 9: Bridge combined with the MTMD system at the section $x = x_{bl}$ under train loads.

An imaginary composite box girder bridge was selected, and its cross-sectional dimensions are illustrated in Figure 10. The diaphragms were arranged at both ends, and the shear studs were distributed close and spaced evenly. Thus, we assume the shear connection stiffness ρ_{sh} (actually the shear force per interface [37]) to be linearly elastic, uniform, and constant. Considering Ollgaard's nonlinear load-slip relationships [42], the load-slip relationship of each shear stud was the secant stiffness at 40% of the ultimate strength [43], as $\rho_{sh} = 10\,\text{kN/mm}^2$. Young's modulus of steel and concrete was $E_s = 2.06 \times 10^5\,\text{MPa}$ and $E_c = 3.86 \times 10^4\,\text{MPa}$, respectively. In addition, Poisson's ratios are $\mu_s = 0.3$ and $\mu_s = 0.2$, respectively. Therefore, the first-order natural frequency obtained from the eigenvalue analysis was 3.98 Hz, with the equivalent composite damping ratio ξ_b considered to be 2.98% [44]. The corresponding vibration mode was vertical bending, selected as the module to be controlled. The MTMD device was installed on the box girder bridge's interior at its midspan (where the dynamic response is the largest in the first mode) with a uniformly distributed mass ratio of 0.7%.

As the train operates at a uniform speed V, forming a series of regular axle loads, they might well exert a periodic dynamic effect on the bridge. We assume that the interval between moving train loads d_v and its cycle should be d_v/V. When it corresponds to the nth-order natural frequency of the bridge or i times of the harmonic cycle, resonance will occur. According to Frýba [45], the critical speed V_{re} (km/h) can be expressed as

Table 1: The ICE3 train's parameters.

Parameters	Unit	Value
m_{vc}	kg	48000
$J_{vc\theta}/J_{vc\varphi}/J_{vc\psi}$	kg·m^2	115000/2700000/2700000
m_{vt}	kg	3200
$J_{vt\theta}/J_{vt\varphi}/J_{vt\psi}$	kg·m^2	3200/7200/6800
m_{vw}	kg	2400
$J_{vw\theta}$	kg·m^2	1200
$k_{v1a}/k_{v1h}/k_{v1v}$	kN/m	18000/6000/2080
$c_{v1a}/c_{v1h}/c_{v1v}$	kN·s/m	0/0/10
$k_{v2a}/k_{v2h}/k_{v2v}$	kN/m	480/480/800
$c_{v2a}/c_{v2h}/c_{v2v}$	kN·s/m	20/60/12
d_{v1}	M	21.075
d_{v2}	M	23.575
b_{v1}	M	1
b_{v2}	M	0.95
h_{v1}	M	0.8
h_{v2}	M	0.3
h_{v3}	M	0.14
h_{v4}	M	2.466

$$V_{re} = \frac{3.6 f_b}{i} \cdot d_v \, (i = 1,2,3\ldots), \tag{19}$$

where f_b (Hz) is a certain natural frequency of the bridge (in this study, it is selected as the fundamental frequency) and d_v (m) is the fixed wheelbase.

Let $i = 2$, and the operation speed is $V \approx 180\,\text{km/h}$.

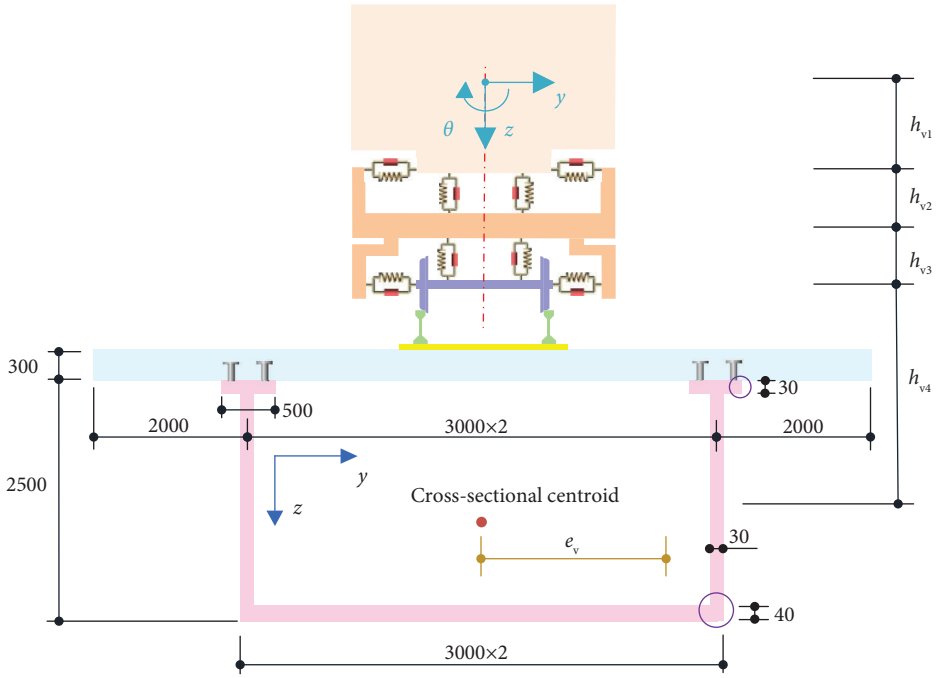

FIGURE 10: The composite box girder bridge along the monoline (unit: mm).

4.2. Comparison and Selection of the Optimization Algorithm. In most cases, closed-form expressions from Den Hartog [46] were utilized in this study to simplify the process of the numerical simulation, appropriate for the optimization of an SDOF (single degree offreedom) TMD with undamped SDOF structures subjected to harmonic excitations. Thus, the optimum tuning frequency ratio β_{ti} and the optimum damping ratio ξ_{ti} of a TMD are expressed, respectively,

$$\begin{aligned} \beta_{ti,\mathrm{opt}} &= \frac{1}{1+\mu_{ti}}, \\ \xi_{ti,\mathrm{opt}} &= \sqrt{\frac{3\mu_{ti}}{8(1+\mu_{ti})^3}}, \end{aligned} \tag{20}$$

where μ_{ti} is the mass ratio of a single TMD, defined as $\mu_{ti} = m_{ti}/m_b$ $(i = 1,2,3,\ldots,n)$, and m_{ti} and m_b are the mass of an individual TMD and the composite girder bridge, respectively.

The expressions of Den Hartog or Warburton [47] can be utilized as the initial parameters of optimization in this study. However, Warburton's expressions only apply to SDOF structures subjected to white noise excitations, which is not suitable for this study. Thus, the optimum tuning frequency $\omega_{ti,\mathrm{opt}}$, stiffness $k_{ti,\mathrm{opt}}$, and damping $c_{ti,\mathrm{opt}}$ of a single TMD can be calculated as follows:

$$\omega_{ti,\mathrm{opt}} = \beta_{ti,\mathrm{opt}}\omega_{b1}, \tag{21}$$

$$\begin{aligned} k_{ti,\mathrm{opt}} &= m_{ti}\omega_{ti,\mathrm{opt}}^2, \\ c_{ti,\mathrm{opt}} &= 2\xi_{ti,\mathrm{opt}}m_{ti}\omega_{ti,\mathrm{opt}}, \end{aligned} \tag{22}$$

where ω_{b1} is the bridge's angular frequency in the first order, $\omega_{b1} = 2\pi f_{b1}$.

For most of the simple structures, the mode superposition method is appropriate for solving their dynamic responses. Undoubtedly, its dynamic amplification factor can be treated as the optimization objective function during the optimization for the TMD. The advantage of this approach is that only several key modes need tuning for vibration control and that the solution can be obtained through general optimization algorithms. However, in this study, the proposed approach was established for the purpose of higher analysis accuracy, the downside of which was more difficult to optimize the parameters of MTMDs. Obviously, almost all simple optimization algorithms are not a good choice for the optimal design, especially under train-bridge interactions. For another, the time-varying coupling system itself is rather complex in terms of the optimization design. So objective functions can only take the maximum vertical responses after all time steps of iteration, which are nondifferentiable and classified as implicit function optimization.

For the better optimization and comparison, three trains $(n_v = 3)$ passed over the composite box girder bridge, an individual TMD $(n = 1)$ considered a spring-mass-damping system. Therefore, taking the maximum acceleration of the bridge as an objective function, the final optimization problem is simplified as the following expressions:

$$\begin{cases} \min \quad \ddot{v}_{bl,\max}(\mu_t, \beta_{ti}, \xi_{ti}) \\ s.t.\ \mu_t = 0.02; \\ \beta_{ti} \in [0.8, 2.2]; \\ \xi_{ti} \in (0, 0.5]. \end{cases} \tag{23}$$

At present, numerical optimization methods, such as ergodic search methods, are reasonable for calculations, as the classical closed-form expressions of TMD above are always limited in practice.

In a TMD/MTMD system, the pattern search method (PSM), particle swarm optimization (PSO), and genetic algorithm (GA) were selected as optimization methods separately for programming in MATLAB 2021 embedded with the optimization toolbox. The specific implementation is to set the initial TMD's/MTMD's parameters $\{\mu_{t0}, \beta_{t0}, \xi_{t0}\}$, and their boundaries are included within a certain range in equation (21). In the end, optimum TMD/MTMD parameters could be obtained. More details about the procedures are shown in Figure 11.

Under the same initial conditions, three different algorithms above were used to optimize μ_t, frequency ratio β_{t1}, and damping ratio ξ_{t1} of a TMD system. The optimization results of these algorithms are listed in Table 2, and the optimization results are illustrated in Figure 12.

In light of efficiency of optimization, PSM and PSO are better than GA in searching the optimal value, but the optimization time of PSM was significantly reduced to the minimum out of these because the initial points were calculated by closed-form expressions of Den Hartog, accelerating the speed of converging to the optimal value points during the search process. Instead, from the optimization results, the computational efficiency of GA was still the lowest and was not suitable for the optimization of this strongly coupled time-varying system.

The goal of the optimization algorithm is to make the results as close to the optimal value as possible with less computation and time. Therefore, the subsequent research in this study adopted PSM combined with closed-form expressions of Den Hartog as the initial point, which saved a great deal of time and facilitated optimization.

5. Factors Affecting Vibration Control

5.1. The Mass Ratio. To lower the difficulty of optimization and reflect the effect of the mass ratio, the parameters of both trains and the simply supported composite box girder bridge remained consistent with those described in Section 4.1, while the MTMD system was simplified to a TMD system, i.e., $n = 1$, installed inside the composite box girder bridge at its midspan. The range of the mass ratio μ_t varied from 0.005 to 0.05 with an interval of 0.005. The corresponding optimum tuning frequency ratio $\beta_{t,\mathrm{opt}}$ and damping ratio $\xi_{t,\mathrm{opt}}$ were obtained by PSM. In this case, the maximum acceleration and deflection of the bridge at its midspan were regarded as the optimization objective functions, respectively. The optimization problem was finally simplified to the following expression:

$$\begin{cases} \min \quad \nu_{\mathrm{bl,max}}(\mu_t, \beta_{ti}, \xi_{ti}) \text{ or } \ddot{\nu}_{\mathrm{bl,max}}(\mu_t, \beta_{ti}, \xi_{ti}), \\ s.t.\ \mu_t = [0.005{:}\ \Delta\mu_t = 0.005{:}\ 0.05]; \\ \beta_{ti} \in [0.8, 2.2]; \\ \xi_{ti} \in (0, 0.5]. \end{cases} \tag{24}$$

After parameter optimization by PSM, the maximum dynamic response in the midspan cross section under different mass ratios is shown in Figure 13.

The results indicate that the vertical dynamic responses of the composite girder bridge at its midspan decrease with an increase in the mass ratio μ_t and that the vibration-damping effect of the TMD system gradually enhanced. However, when the TMD mass ratio reaches 3.5% or more, the trend of acceleration is slightly different from deflection. The former is not obvious; the latter, nevertheless, is still decreasing slightly.

From a great deal of earlier research, the mass ratio μ_t of the MTMD system usually lies within the range of 1%–5% [48–52]. The lighter the mass, the more difficult it is for the MTMD system to achieve the ideal damping effect. On the other hand, if the mass is too heavy, like static loading, the dynamic characteristics of the bridge and its mechanical behaviors would change. Afterward, for large structures such as the railway bridge (the mass itself is quite large), it is extremely difficult to obtain a mass ratio of more than 3%. Therefore, the design of MTMDs should be taken into a comprehensive consideration of the economy, bearing capacity of the composite box girder bridge, and vibration-damping effect of MTMDs. Thus, based on the consideration above, in the following research, the mass ratio μ_t of the MTMD system will be maintained at approximately 2%.

5.2. Train's Number. Given the limited internal space of the composite box girder bridge, inconvenient installation, and maintenance of an individual TMD, the MTMD system was only composed of three TMDs, which were evenly distributed in the transverse direction. During the optimization process, every small TMD had the same mass ratio of 0.7% and remained constant but not the same frequency β_{ti} and damping ratio ξ_{ti}. The parameters of both trains and the simply supported composite box girder bridge remained consistent with those in Section 4.1, while the number of trains varied, i.e., $n_v = 1$, 3, 5, and 8, respectively. In this case, the maximum acceleration and deflection of the bridge at its midspan were regarded as the optimization objective functions, respectively. The optimization problem was finally simplified to the following expression:

$$\begin{cases} \min \quad \nu_{\mathrm{bl,max}}(\mu_t, \beta_{ti}, \xi_{ti}) \text{ or } \ddot{\nu}_{\mathrm{bl,max}}(\mu_t, \beta_{ti}, \xi_{ti}) \\ s.t.\ \mu_t = 3 \times 0.007 = 0.021; \\ \beta_{ti} \in [0.8, 2.2]; \\ \xi_{ti} \in (0, 0.5]. \end{cases} \tag{25}$$

After parameter optimization by PSM, the optimum tuning frequency ratio β_{ti} and damping ratio ξ_{ti} of MTMDs and the maximum dynamic response of the bridge at its midspan $\ddot{\nu}_{\mathrm{bl,max}}$ and $\nu_{\mathrm{bl,max}}$ are demonstrated in Table 3. The vertical accelerations and deflections in both the time history and frequency domain are displayed in Figures 14–21.

Thus, it can be viewed from the above that the interaction between every train and the composite girder bridge will be more obvious due to the increase in the number of trains,

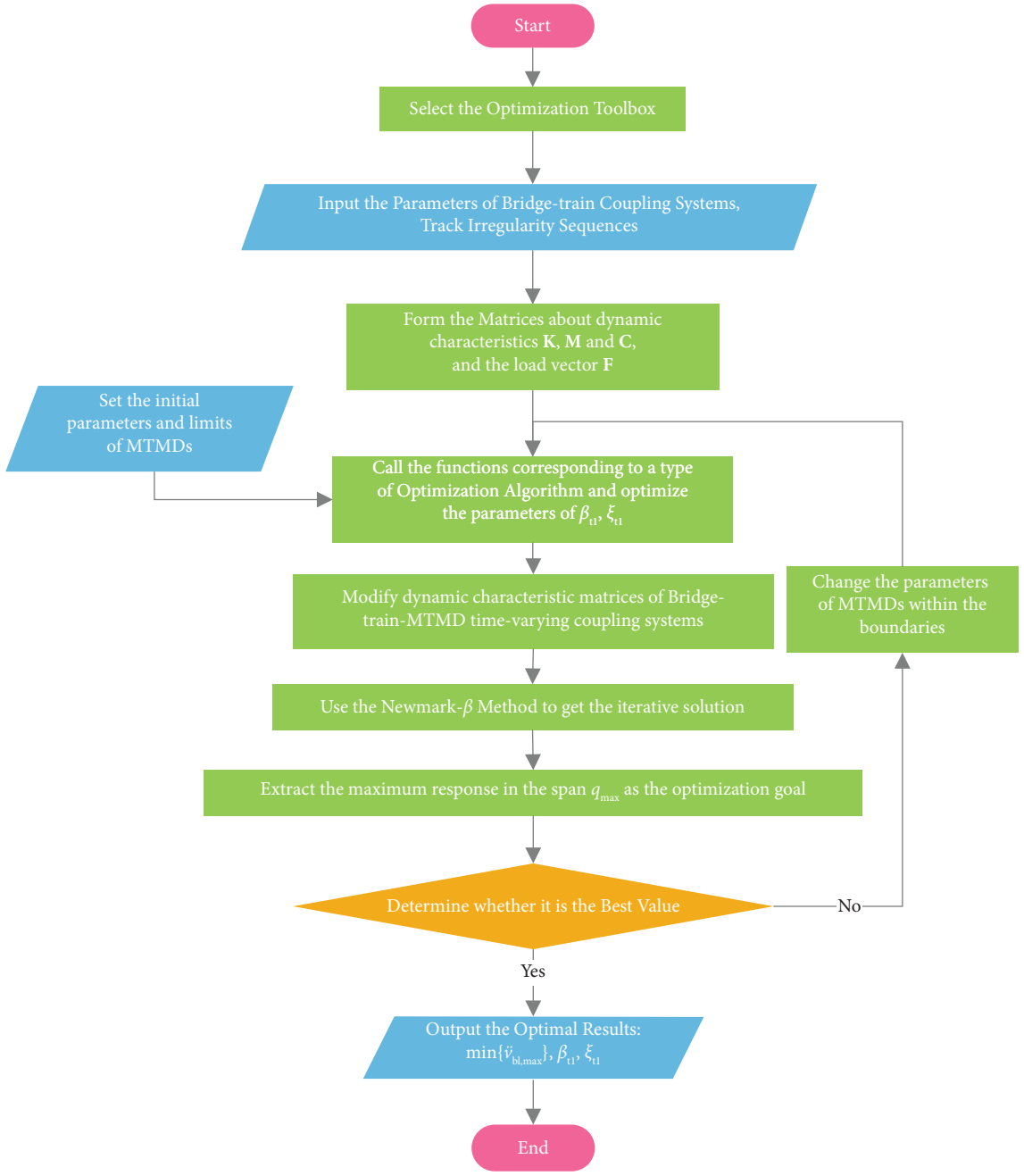

Figure 11: Optimization design flowchart of MTMDs.

and vertical dynamic responses of the bridge are also amplified with the superposition of continuous periodic excitations from the trains. For example, vertical acceleration and deflection were increased to 1.7059 m/s^2 and 5.867 mm, respectively.

However, due to the coupling effect and the assumption of the wheel-rail rolling contact, the bridge's natural frequency is always changing when the train runs on it, because the mass of wheel sets is added to the bridge so that the dynamic peak in the frequency domain does not correspond to the first-order frequency of the bridge but is slightly smaller. Even so, MTMDs still work as they would first resonate with the excitation to suppress the vibration of the corresponding mode of the composite girder bridge and avoid resonance after tuning.

Figure 22 shows vertical deflection and acceleration damping ratios of the composite box girder bridge at its midspan regarding different train's numbers within the whole time trains pass. When the number is increased from 1 to 3, the vibration damping ratio for the vertical acceleration of the bridge at its midspan reduces from 34.39% to 33.52% and for the vertical deflection from 1.62% to 1.51%. Although they are both reduced, yet not much, they tend to be toward stability. When the number is 3, the vibration damping ratios of its vertical acceleration and deflection are close to the minimum. When the number increases from 3 to

Table 2: Optimization results.

The number of trains	Iteration/generation (in GA)	$\beta_{t,\mathrm{opt}}$	$\xi_{t,\mathrm{opt}}$	The best value $\ddot{v}_{\mathrm{bl,max}}$ (m/s^2)	Time (s)
PSM	44	1.183297	0.01000	0.7050	48.481
PSO	33	1.183296	0.01000	0.7050	270.955
GA	60	1.183303	0.01003	0.7051	952.053

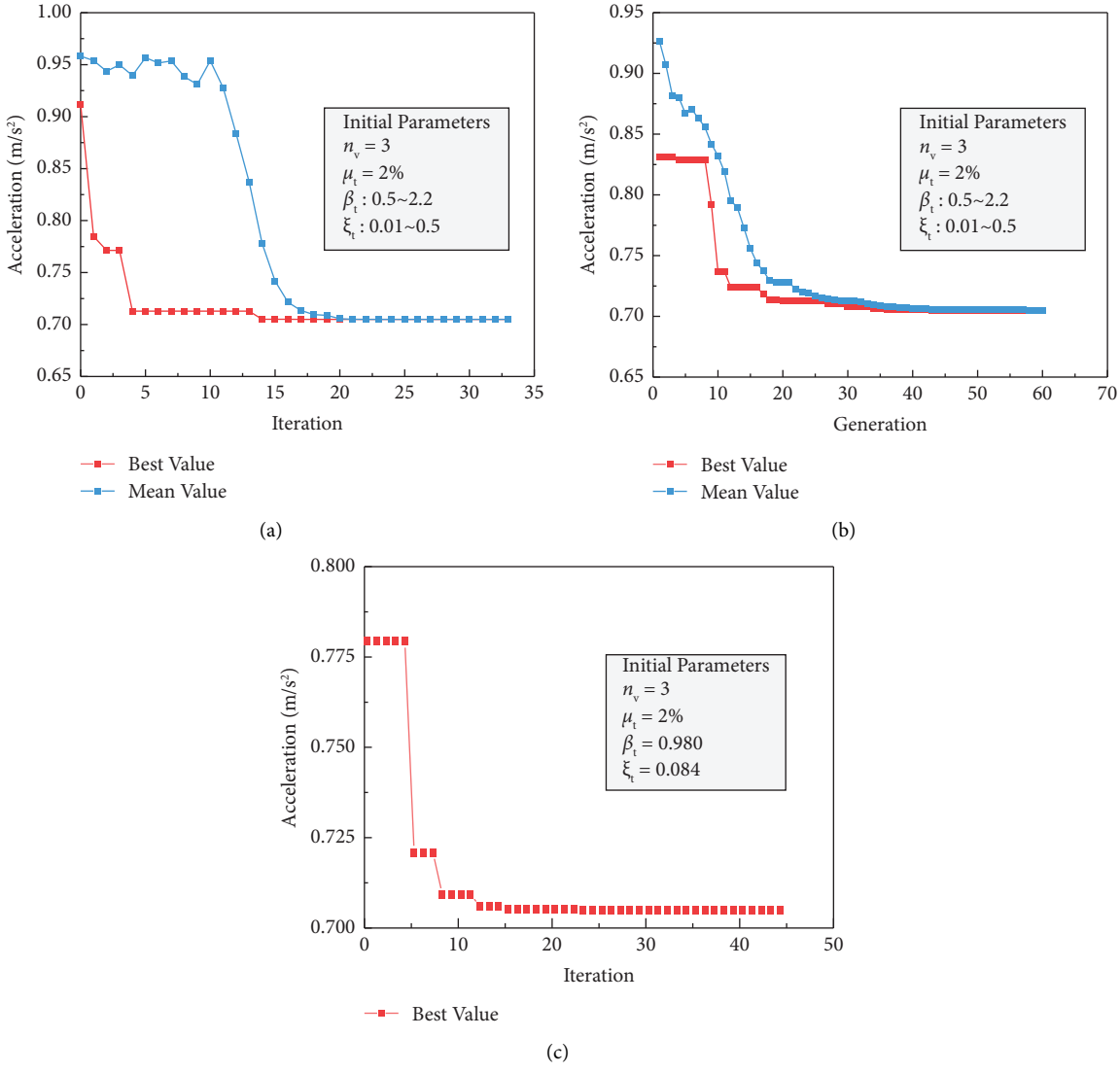

Figure 12: Optimization process of three algorithms: (a) particle swarm optimization; (b) genetic algorithm; (c) pattern search method.

5, the vibration damping ratio for the vertical acceleration increases to 40.98% and for the vertical deflection to 14.36%. When the number of trains is 8, the vibration damping ratios for vertical acceleration and deflection become maximum, which are 43.02% and 16.53%, respectively.

In general, the vibration damping ratios of vertical acceleration and deflection of the bridge at its midspan increased as the number of trains increased. When the number was increased from 1 to 8, the resonance effect became more obvious. This made the vibration damping ratios of MTMDs for the vertical acceleration and deflection increase by 8.63% and 14.91%, respectively, whereas the dynamic characteristics of the composite girder bridge do not change in nature.

In addition, the vibration-damping effect of MTMDs for vertical acceleration is still better than that of vertical deflection, because MTMDs themselves only reduce the dynamic deflection of a structure, and static deflection accounts for a large proportion. In other words, the response of vertical deflection was particularly concentrated in the range of low frequency (0-1 Hz), but MTMDs can be

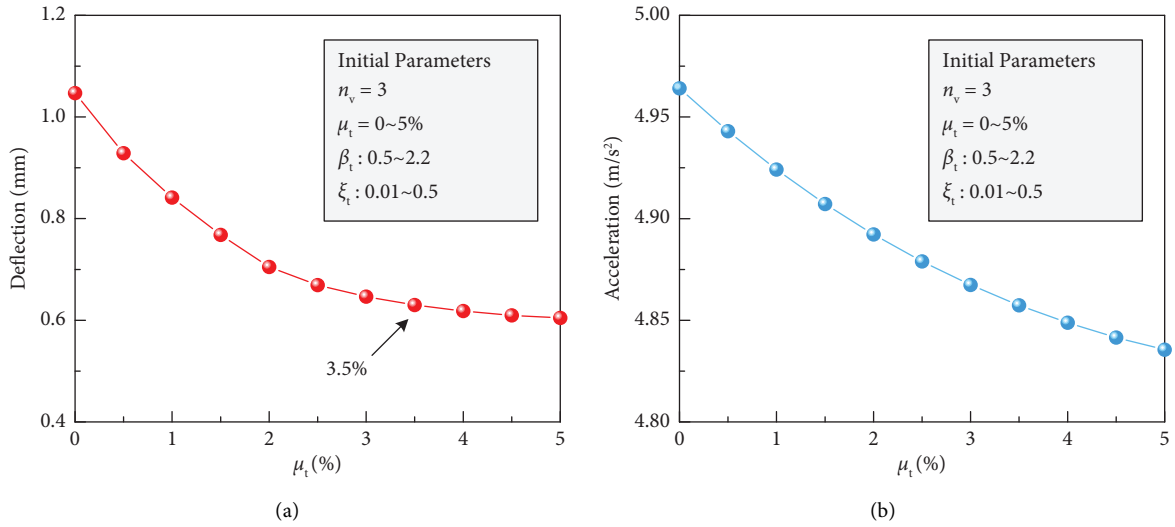

Figure 13: Influence of the mass ratio.

Table 3: Influence of the train's number.

The number of trains		1	3	5	8
$\ddot{v}_{bl,\max}$ (m/s^2)	Without MTMDs	0.6641	1.0469	1.6470	1.7059
	With MTMDs	0.4457	0.6960	0.9721	0.9721
Acceleration damping ratio		34.39%	33.52%	40.98%	43.02%
$\beta_{ti,\text{opt}}$		1.0696, 1.0696, 1.0696	1.1854, 1.1898, 1.1918	1.1734, 1.1734, 1.1734	1.1734, 1.1734, 1.1734
$\xi_{ti,\text{opt}}$		0.01, 0.01, 0.01	0.01, 0.01, 0.01	0.01, 0.01, 0.01	0.01, 0.01, 0.01
$v_{bl,\max}$ (mm)	Without MTMDs	2.882	4.964	5.718	5.867
	With MTMDs	2.819	4.889	4.897	4.897
Deflection damping ratio		1.62%	1.51%	14.36%	16.53%
$\beta_{ti,\text{opt}}$		0.7440, 0.7440, 0.7440	1.2514, 1.2514, 1.2514	1.1860, 1.1480, 1.1480	1.1860, 1.1480, 1.1480
$\xi_{ti,\text{opt}}$		0.01, 0.01, 0.01	0.01, 0.01, 0.01	0.01, 0.01, 0.01	0.01, 0.01, 0.01

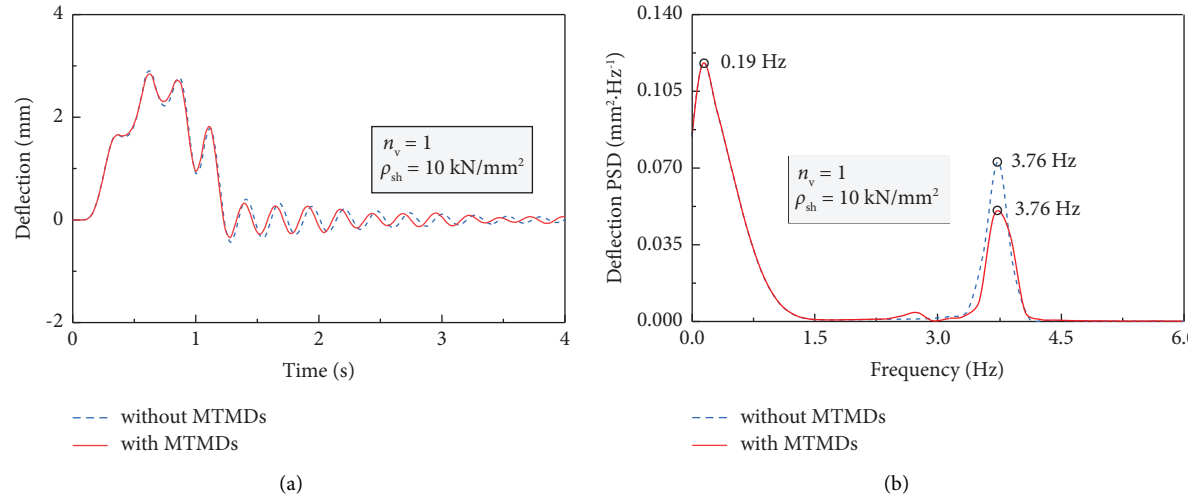

Figure 14: Vertical deflection of the bridge at its midspan when $n_v = 1$: (a) time history; (b) spectral power density.

brought into play only when their frequencies fall in or near a certain frequency of the bridge, so its vertical deflection would not be reduced so much.

5.3. Interface Slip. As illustrated above, the MTMD system was still composed of three TMDs, which were evenly distributed in the transverse direction. During the

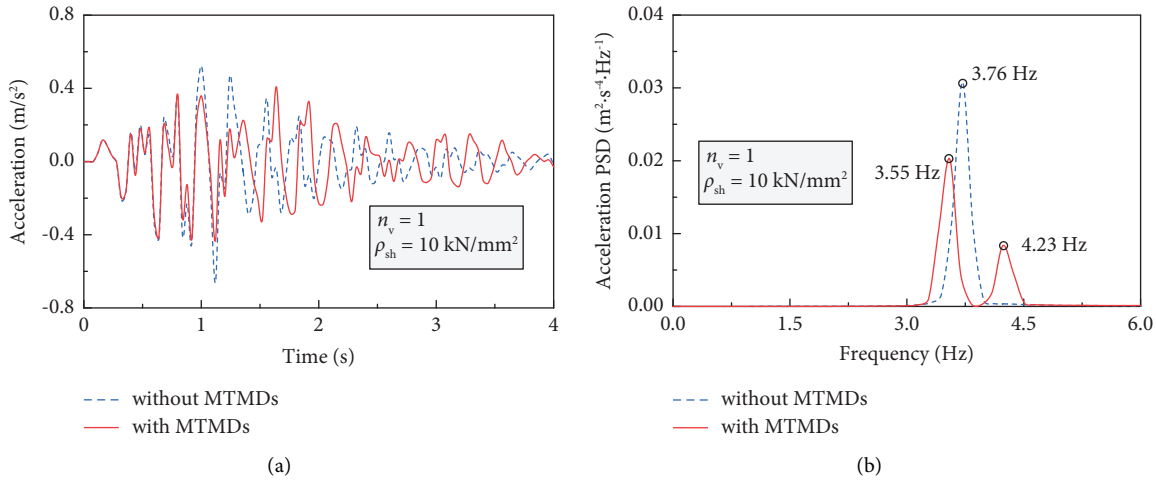

FIGURE 15: Vertical acceleration of the bridge at its midspan when $n_v = 1$: (a) time history; (b) spectral power density.

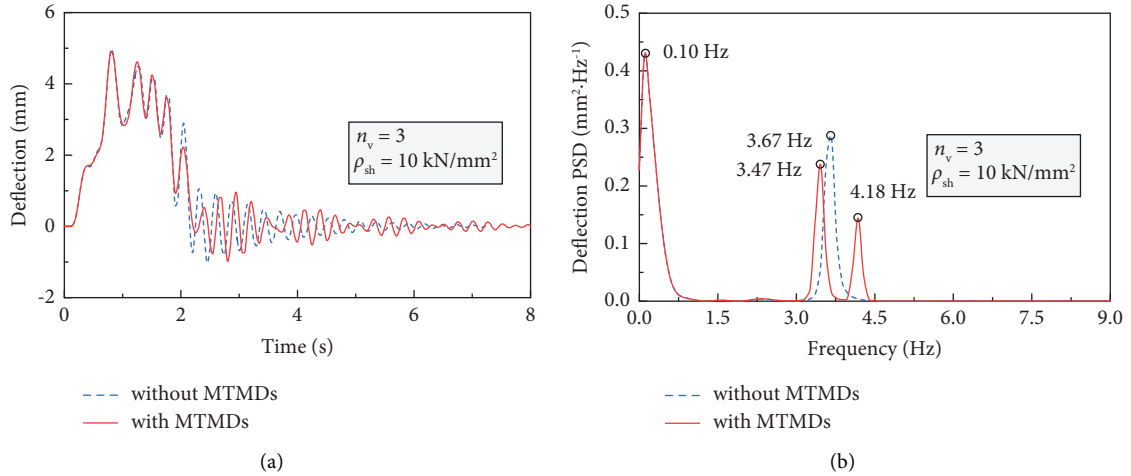

FIGURE 16: Vertical deflection of the bridge at its midspan when $n_v = 3$: (a) time history; (b) spectral power density.

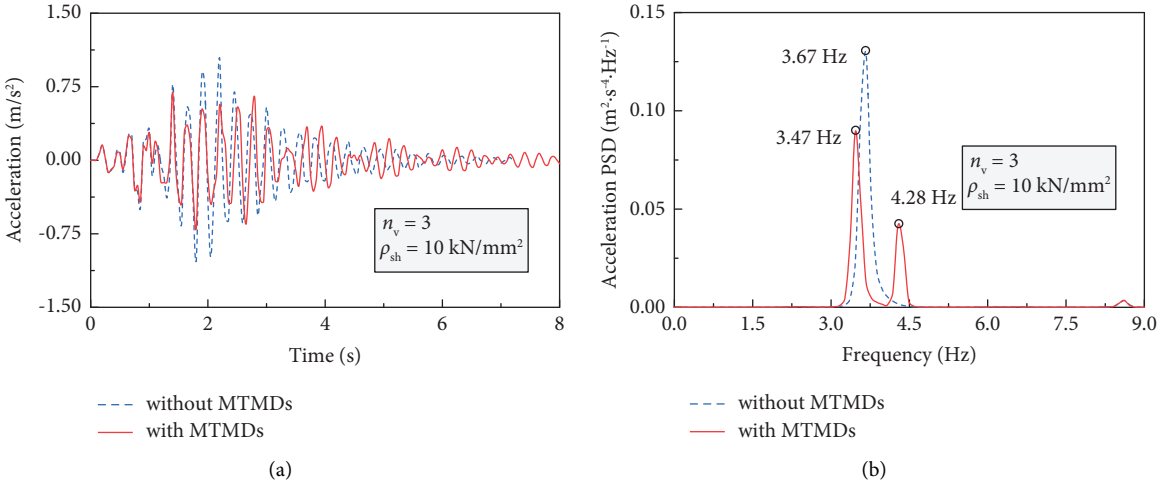

FIGURE 17: Vertical acceleration of the bridge at its midspan when $n_v = 3$: (a) time history; (b) spectral power density.

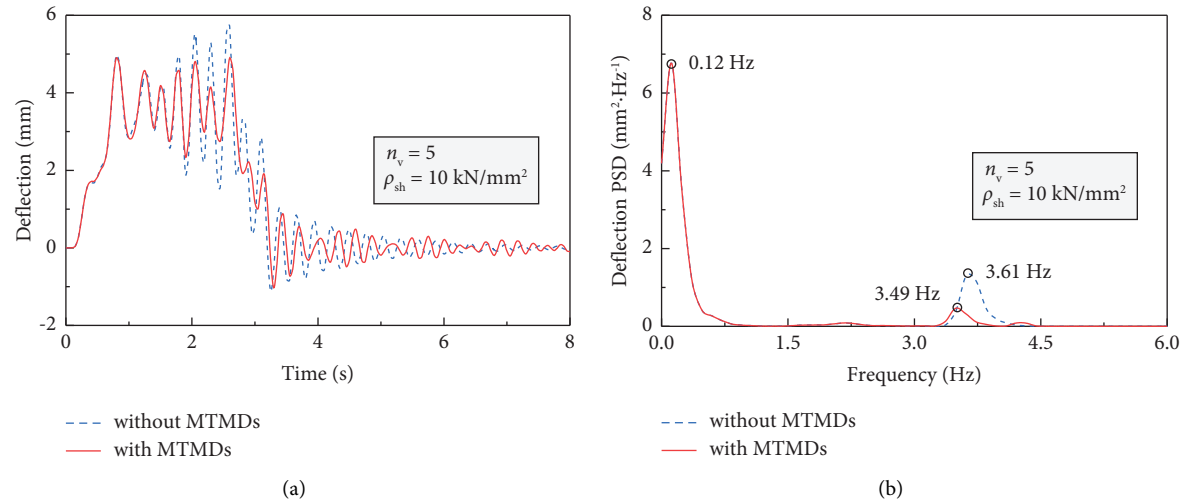

Figure 18: Vertical deflection of the bridge at its midspan when $n_v = 5$: (a) time history; (b) spectral power density.

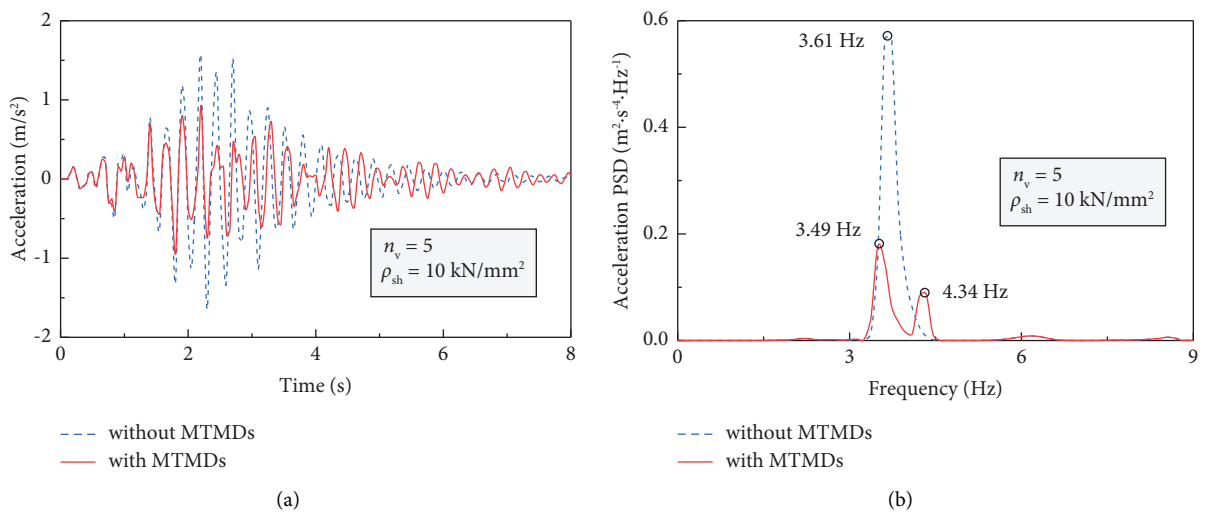

Figure 19: Vertical acceleration of the bridge at its midspan when $n_v = 5$: (a) time history; (b) spectral power density.

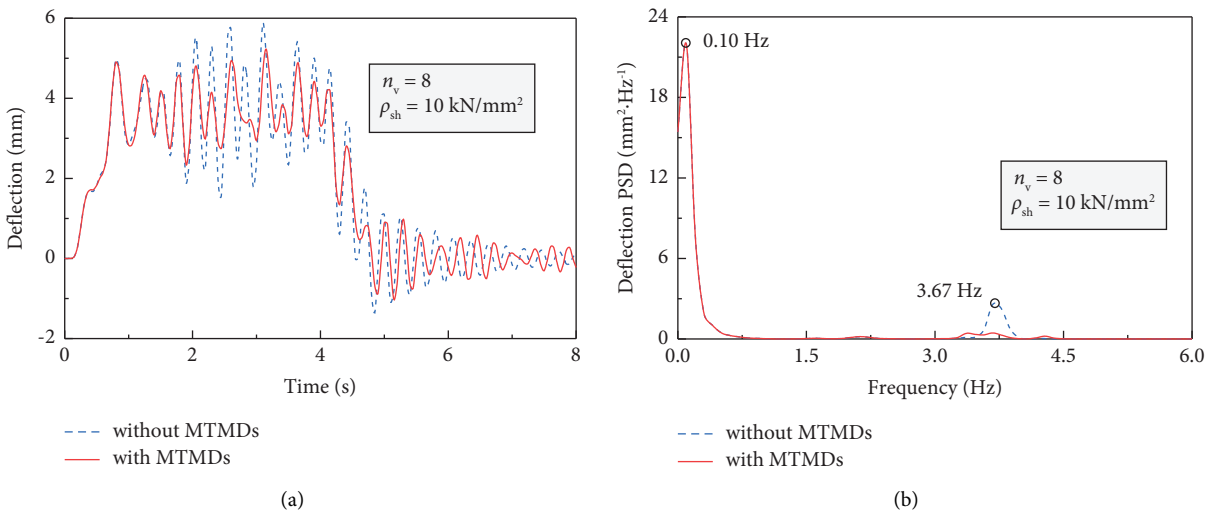

Figure 20: Vertical deflection of the bridge at its midspan when $n_v = 8$: (a) time history; (b) spectral power density.

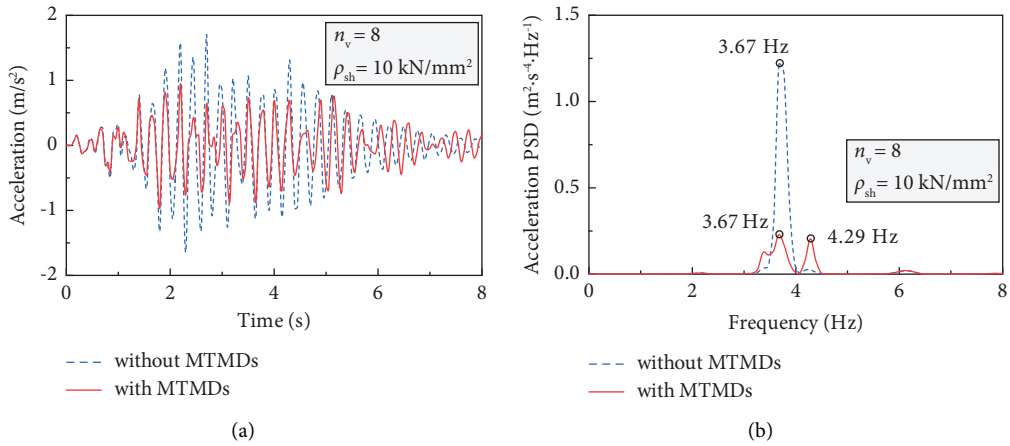

FIGURE 21: Vertical acceleration of the bridge at its midspan when $n_v = 8$: (a) time history; (b) spectral power density.

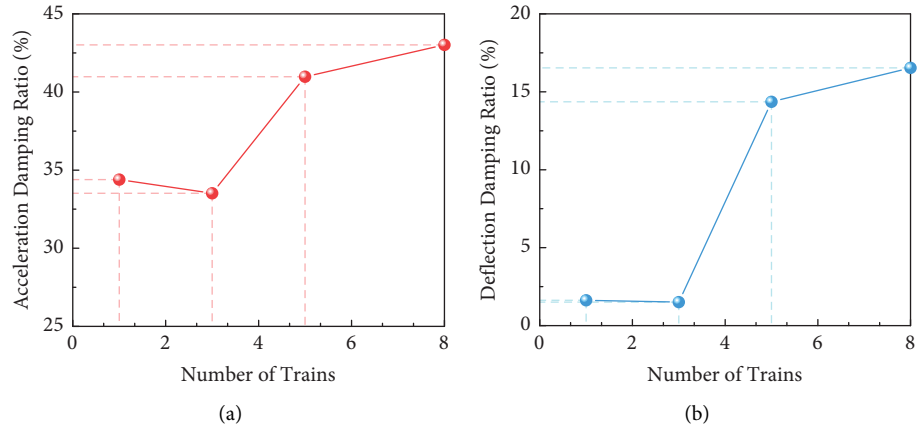

FIGURE 22: The damping ratios of different train numbers.

optimization process, every small TMD had the same mass ratio of 0.7% and remained the same but not the frequency β_{ti} and damping ratio ξ_{ti}. The parameters of trains remained consistent with those in Section 4.1, while the shear connection stiffness of the bridge varied, i.e., $\rho_{sh} = 1\,\text{kN/m}^2$, $\rho_{sh} = 5\,\text{kN/m}^2$, $\rho_{sh} = 10\,\text{kN/m}^2$, and $\rho_{sh} = 100\,\text{kN/m}^2$.

In this case, the maximum acceleration and deflection of the bridge at its midspan were considered the objective functions for optimization. After parameter optimization by PSM, the optimum tuning frequency ratio β_{ti} and damping ratio ξ_{ti} of MTMDs and the maximum dynamic responses of the bridge at its midspan $\ddot{v}_{bl,\max}$ and $v_{bl,\max}$ are demonstrated in Table 4, respectively. The vertical accelerations and deflections in both the time history and frequency domains are displayed in Figures 23–30.

Thus, it is clear from above that the vertical deflection of the bridge at its midspan decreases originally and then increases slightly with the shear connection stiffness ρ_{sh} getting larger, as minimum 5.862 mm and maximum 6.071 mm; the larger the interface connection stiffness, the slighter the increase. However, vertical acceleration increases with an increase in ρ_{sh}, as the maximum is 1.7179 m/s^2; the larger the interface connection stiffness, the slower the increase. The most likely reason is that when a weak shear connection ($\rho_{sh} = 1\,\text{kN/m}^2$) changes to a strong shear connection ($\rho_{sh} = 100\,\text{kN/m}^2$), its fundamental frequency increases slightly, and V_{re} gradually approaches V, so the dynamic responses are amplified, making it close to the condition of resonance. Although vertical acceleration increases to a certain extent as well as vertical deflection, resonance is not prominent due to the large proportion of static (or low-frequency) components. So the overall trend has no significant difference.

Figure 31 shows, respectively, vertical deflection and acceleration damping ratios of the composite box girder bridge at its midspan regarding different shear connection stiffnesses within the whole time trains pass. When ρ_{sh} is $1\,\text{kN/m}^2$, the operation speed of trains V is far from the critical speed V_{re}, the MTMD system has a detuning effect, and the vibration damping ratios decrease to minimum, which are 18.96% and 2.75%, respectively. When ρ_{sh} increases from $1\,\text{kN/m}^2$ to $5\,\text{kN/m}^2$, the damping ratio for the vertical acceleration of the bridge at its midspan increases to 39.69%, and for vertical deflection, it increases to 14.50%, revealing an obvious difference. When ρ_{sh} increases from $10\,\text{kN/m}^2$ to $100\,\text{kN/m}^2$, the vibration damping ratio tends

Table 4: Influence of the interface slip.

ρ_{sh} (kN/mm^2)		1	5	10	100
$\ddot{v}_{bl,max}$ (m/s^2)	Without MTMDs	1.2350	1.6801	1.7059	1.7179
	With MTMDs	1.0008	1.0133	0.9721	0.9286
Acceleration damping ratio		18.96%	39.69%	43.02%	45.95%
$\beta_{ti,opt}$		1.2250, 1.3500, 1.3537	1.1914, 1.1914, 1.1914	1.1734, 1.1734, 1.1734	1.1558, 1.1558, 1.1558
$\xi_{ti,opt}$		0.0100, 0.0256, 0.0725	0.0100, 0.0100, 0.0100	0.0100, 0.0100, 0.010	0.0100, 0.0100, 0.0100
$v_{bl,max}$ (mm)	Without MTMDs	6.071	5.862	5.867	5.898
	With MTMDs	5.904	5.012	4.897	4.794
Deflection damping ratio		2.75%	14.50%	16.53%	18.72%
$\beta_{ti,opt}$		1.4706, 1.4706, 1.4706	1.2714, 1.1725, 1.1313	1.1860, 1.1480, 1.1480	1.2158, 1.0959, 1.1078
$\xi_{ti,opt}$		0.01, 0.01, 0.01	0.01, 0.01, 0.01	0.01, 0.01, 0.01	0.01, 0.01, 0.01

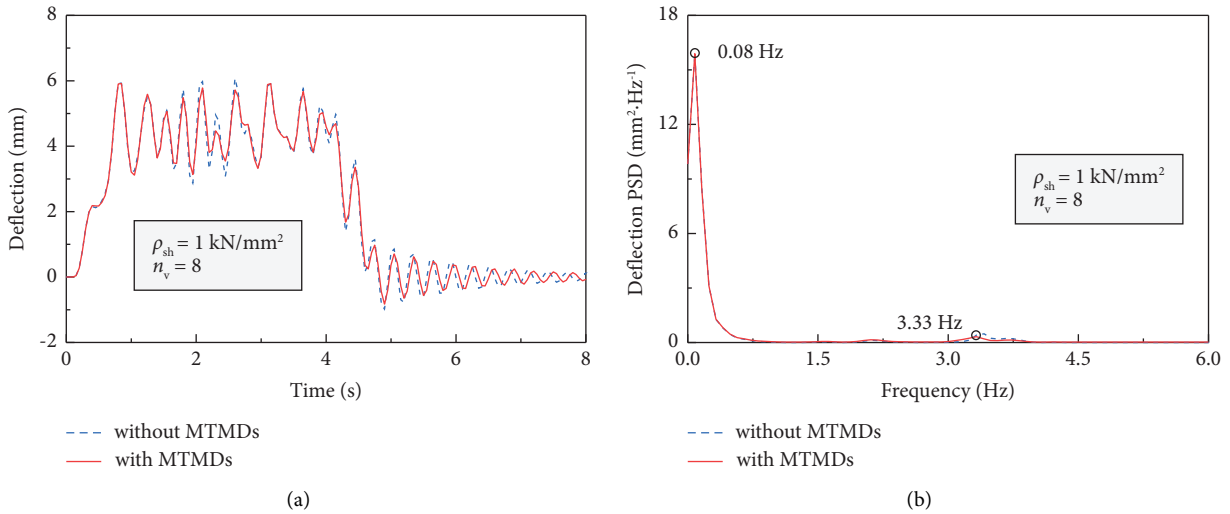

Figure 23: Vertical deflection of the bridge at its midspan when $\rho_{sh} = 1$ kN/m^2: (a) time history; (b) spectral power density.

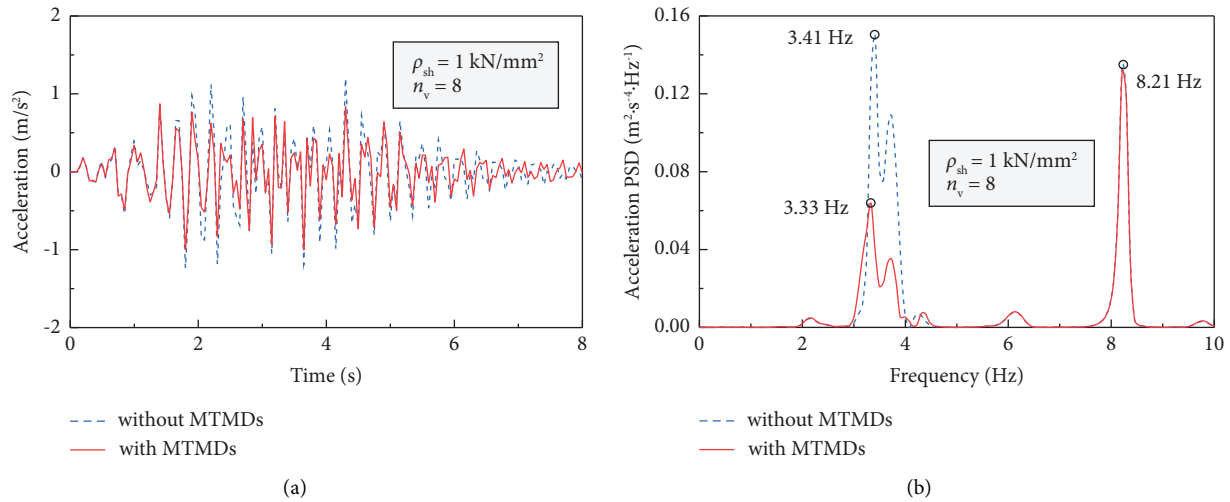

Figure 24: Vertical acceleration of the bridge at its midspan when $\rho_{sh} = 1$ kN/m^2: (a) time history; (b) spectral power density.

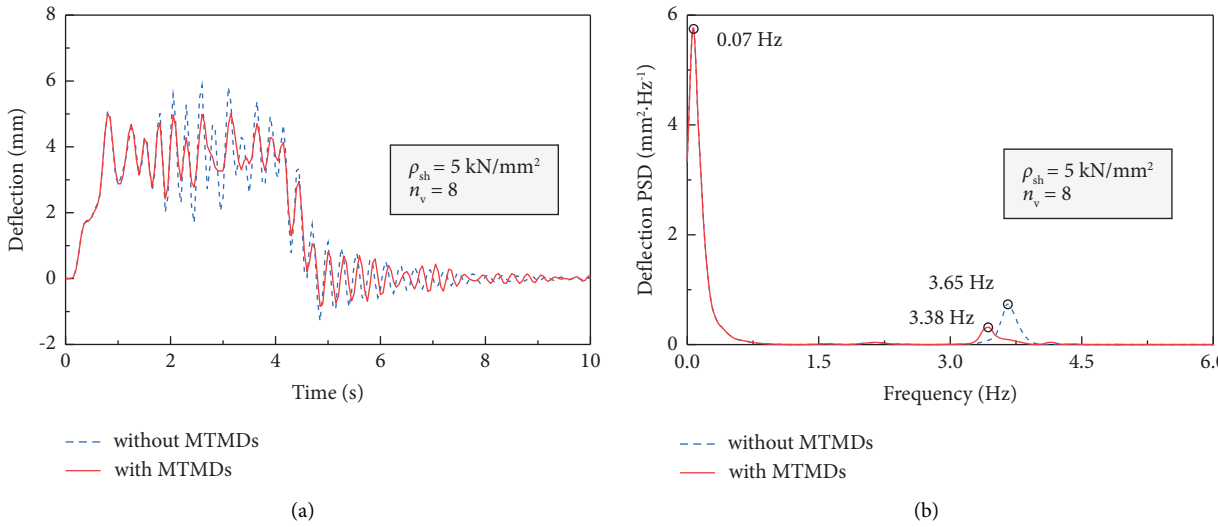

FIGURE 25: Vertical deflection of the bridge at its midspan when $\rho_{sh} = 5\,\text{kN/m}^2$: (a) time history; (b) spectral power density.

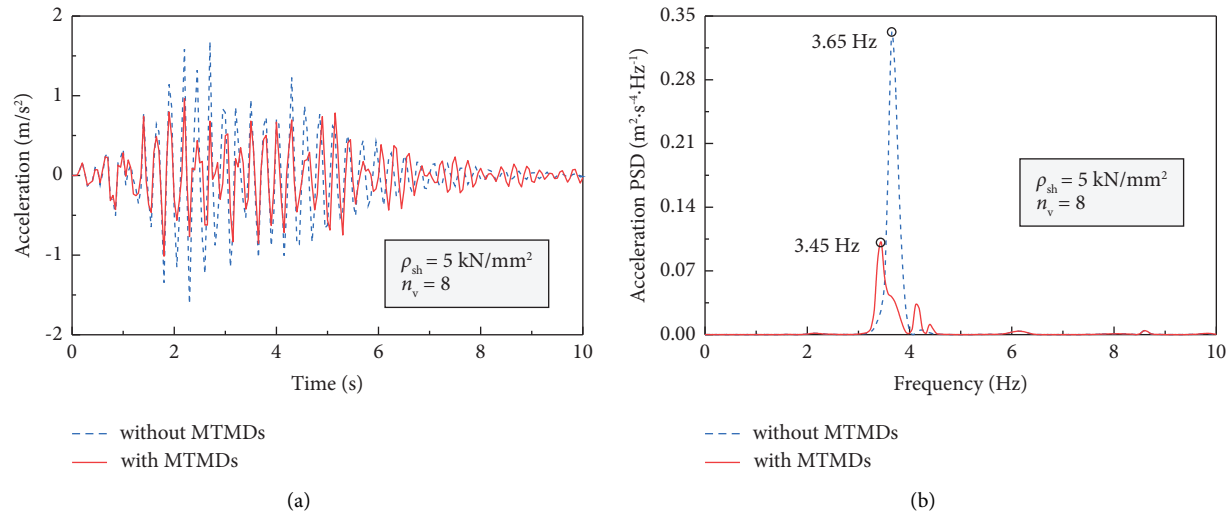

FIGURE 26: Vertical acceleration of the bridge at its midspan when $\rho_{sh} = 5\,\text{kN/m}^2$: (a) time history; (b) spectral power density.

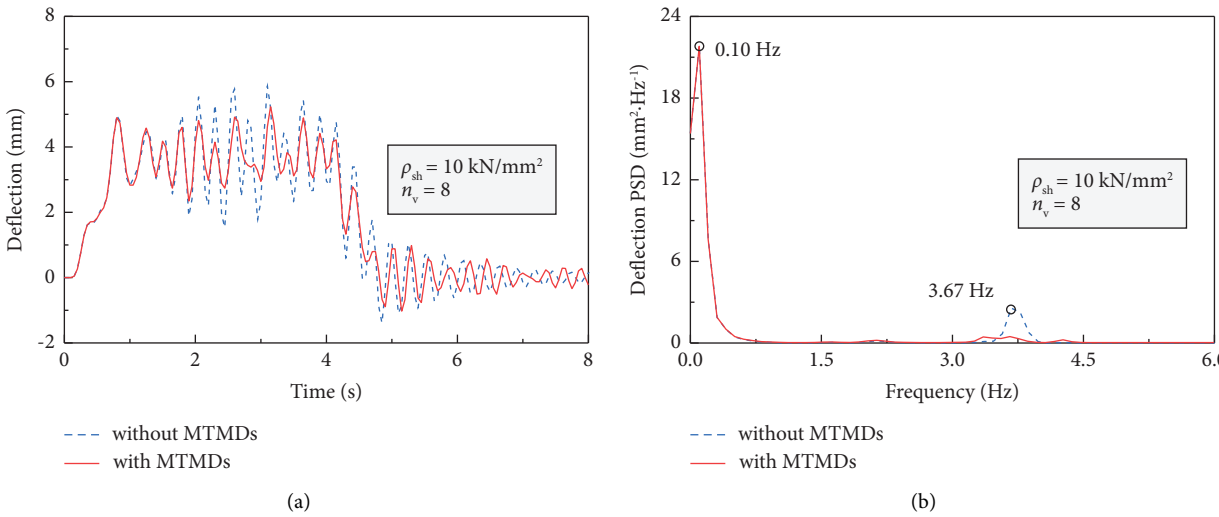

FIGURE 27: Vertical deflection of the bridge at its midspan when $\rho_{sh} = 10\,\text{kN/m}^2$: (a) time history; (b) spectral power density.

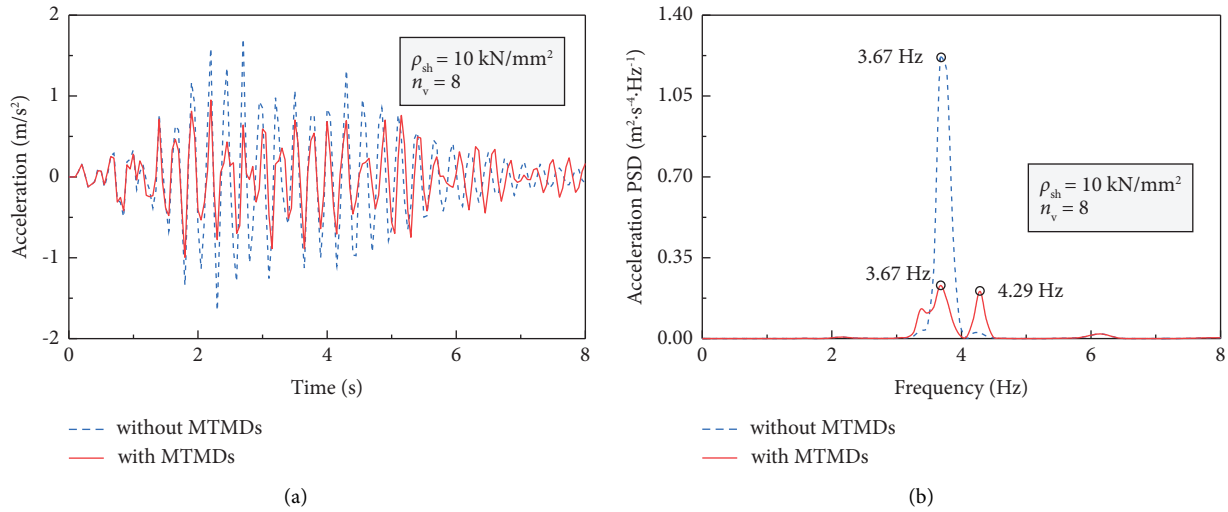

FIGURE 28: Vertical acceleration of the bridge at its midspan when $\rho_{sh} = 10\,\text{kN/m}^2$: (a) time history; (b) spectral power density.

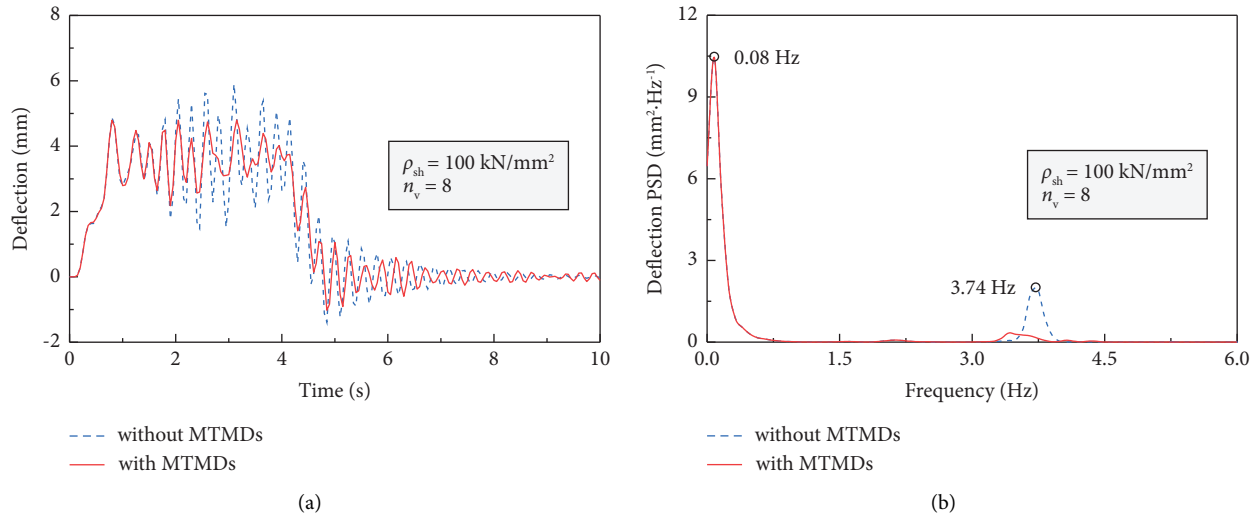

FIGURE 29: Vertical deflection of the bridge at its midspan when $\rho_{sh} = 100\,\text{kN/m}^2$: (a) time history; (b) spectral power density.

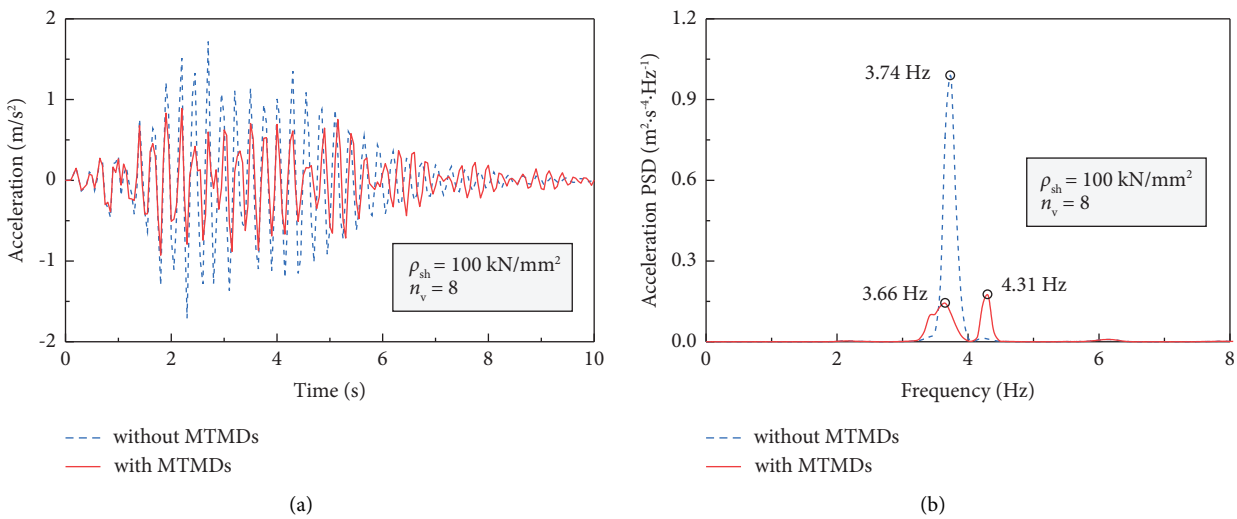

FIGURE 30: Vertical acceleration of the bridge at its midspan when $\rho_{sh} = 100\,\text{kN/m}^2$: (a) time history; (b) spectral power density.

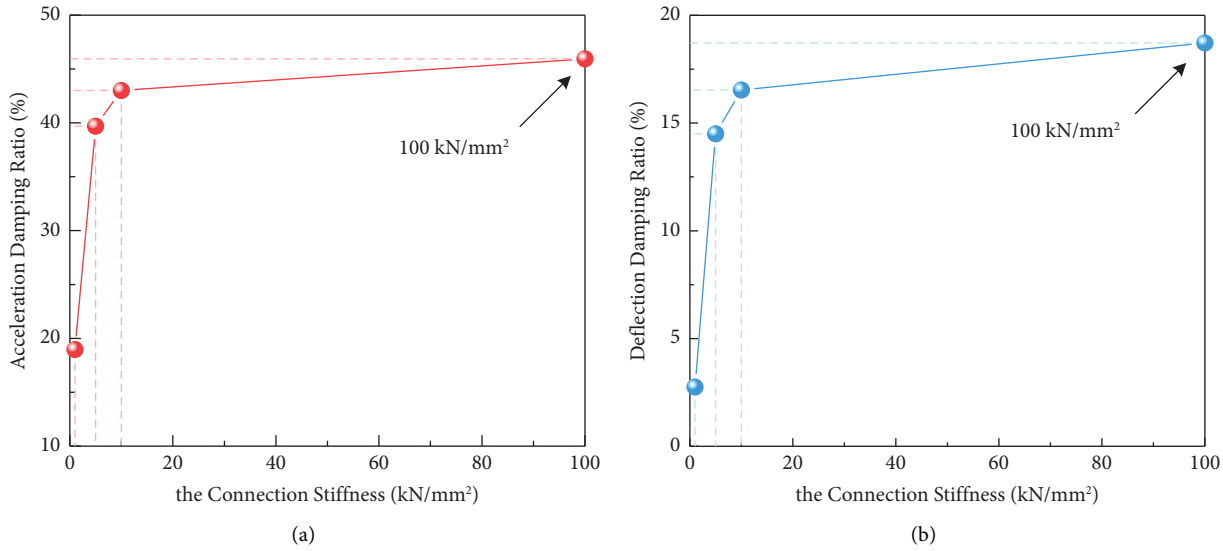

Figure 31: Damping ratios of different shear connection stiffnesses.

Table 5: Influence of shear lag when $2b_c/L = 0.25$

$2b_c/L = 0.25$		No shear lag	With shear lag
$\ddot{v}_{bl,\max}$ (m/s^2)	Without MTMDs	1.6943	1.7039
	With MTMDs	1.0993	1.1349
Acceleration damping ratio		35.12%	33.39%
$\beta_{ti,\text{opt}}$		1.1944, 1.1944, 1.1944	1.2035, 1.2035, 1.2035
$\xi_{ti,\text{opt}}$		0.01, 0.01, 0.01	0.01, 0.01, 0.01
$v_{bl,\max}$ (mm)	Without MTMDs	6.109	6.086
	With MTMDs	5.153	5.135
Deflection damping ratio		15.65%	15.63%
$\beta_{ti,\text{opt}}$		1.8397, 1.0688, 1.0453	1.8492, 1.0541, 1.0692
$\xi_{ti,\text{opt}}$		0.01, 0.01, 0.01	0.01, 0.01, 0.01

Table 6: Influence of shear lag when $2b_c/L = 0.5$

$2b_c/L = 0.50$		No shear lag	With shear lag
$\ddot{v}_{bl,\max}$ (m/s^2)	Without MTMDs	0.9625	1.0167
	With MTMDs	0.6193	0.7700
Acceleration damping ratio		35.66%	24.26%
$\beta_{ti,\text{opt}}$		1.2057, 1.2057, 1.2057	1.2964, 1.2964, 1.2964
$\xi_{ti,\text{opt}}$		0.01, 0.01, 0.01	0.01, 0.01, 0.01
$v_{bl,\max}$ (mm)	Without MTMDs	3.377	3.406
	With MTMDs	2.806	3.189
Deflection damping ratio		16.91%	6.37%
$\beta_{ti,\text{opt}}$		1.8566, 1.0619, 1.0688	1.2250, 1.9750, 1.1000
$\xi_{ti,\text{opt}}$		0.01, 0.01, 0.01	0.198, 0.214, 0.135

to be stable. When ρ_{sh} is 100 kN/m^2, V is the closest to V_{re}, and the resonance effect becomes the most obvious, so the vibration damping ratios of vertical acceleration and deflection reach maximum 45.95% and 18.72%, respectively.

In general, the interface slip reduces the vibration damping ratios of MTMDs for both vertical acceleration and deflection by 26.99% and 15.97%, respectively. The vibration damping ratios of vertical acceleration and deflection of the bridge at its midspan increase as ρ_{sh} becomes larger. In addition, the larger the shear connection stiffness, the slighter the increase. Therefore, the decrease of ρ_{sh} slightly changes the dynamic characteristics of the bridge, making its resonance weaker and even less obvious. Thus, the vibration damping ratio of MTMDs greatly reduces, which, to a certain extent, reflects that it is only suitable for structures under narrow bandwidth excitations.

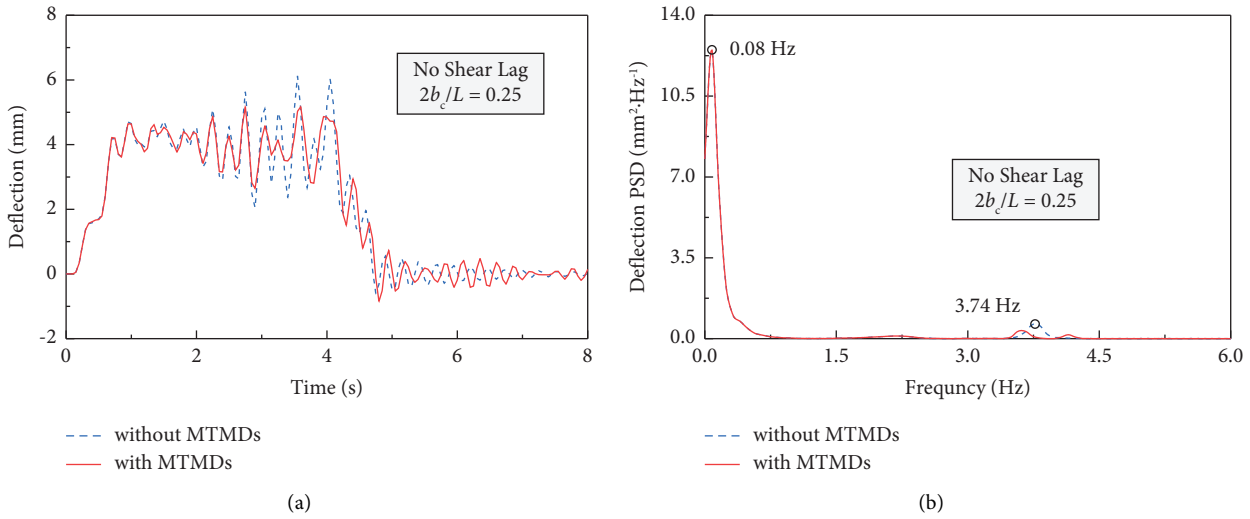

FIGURE 32: Vertical deflection of the bridge at its midspan when $2b_c/L = 0.25$ without shear lag: (a) time history; (b) spectral power density.

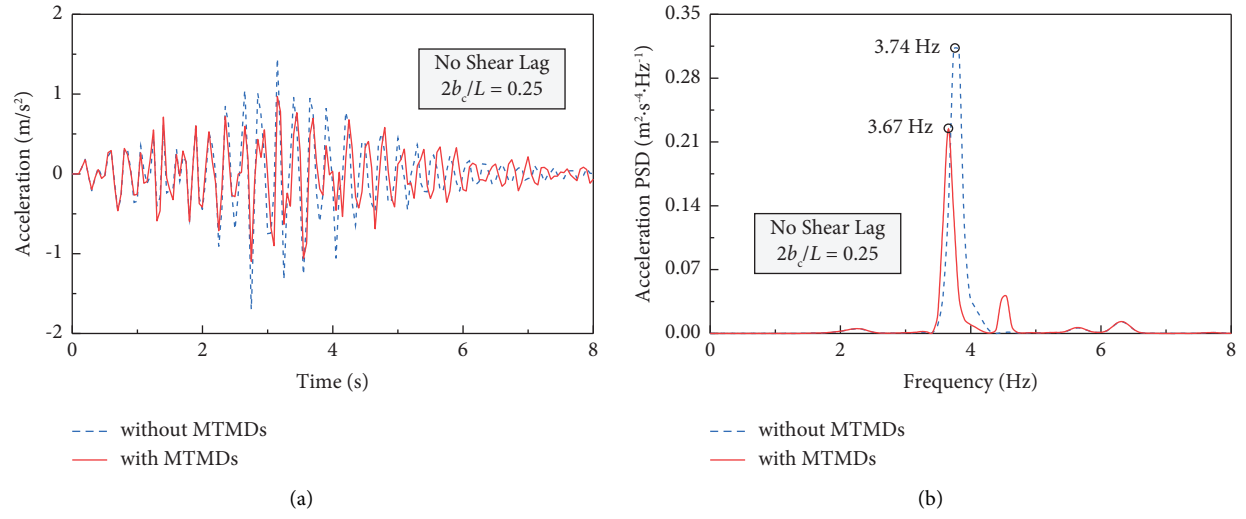

FIGURE 33: Vertical acceleration of the bridge at its midspan when $2b_c/L = 0.25$ without shear lag: (a) time history; (b) spectral power density.

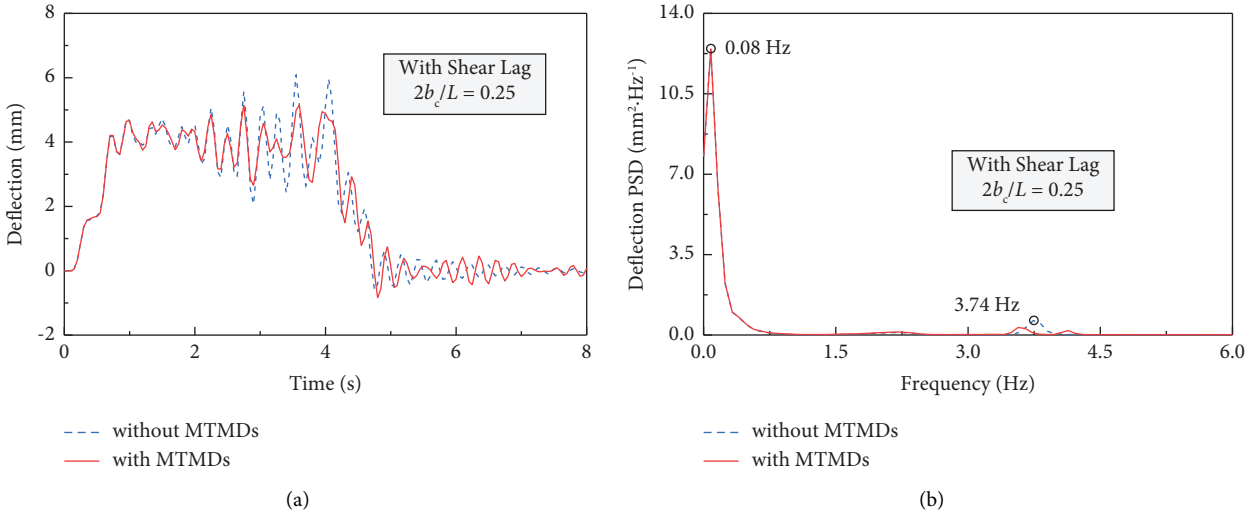

FIGURE 34: Vertical deflection of the bridge at its midspan when $2b_c/L = 0.25$ with shear lag: (a) time history; (b) spectral power density.

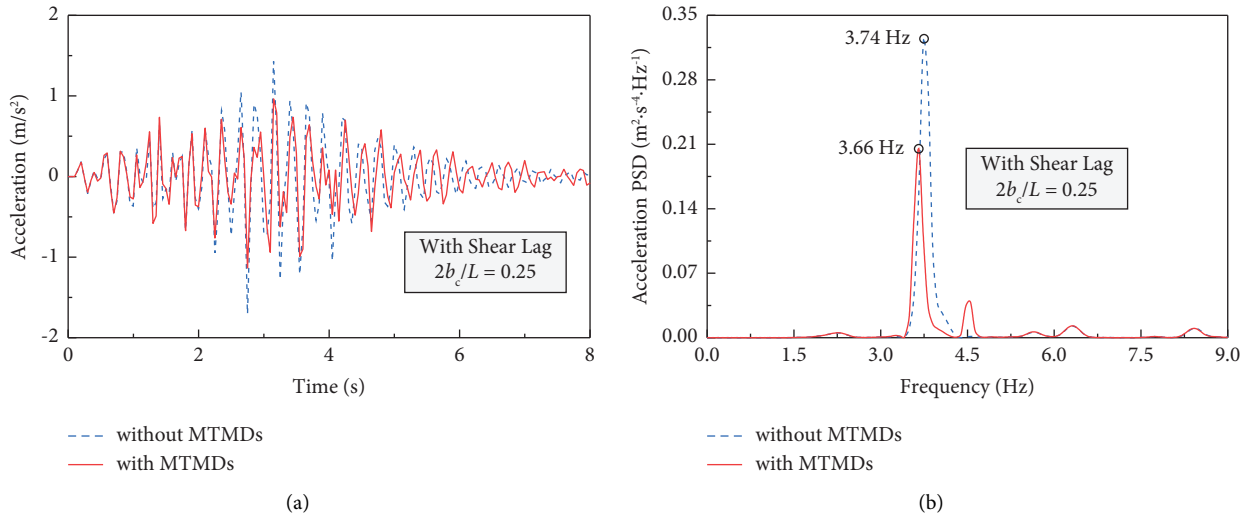

FIGURE 35: Vertical acceleration of the bridge at its midspan when $2b_c/L = 0.25$ with shear lag: (a) time history; (b) spectral power density.

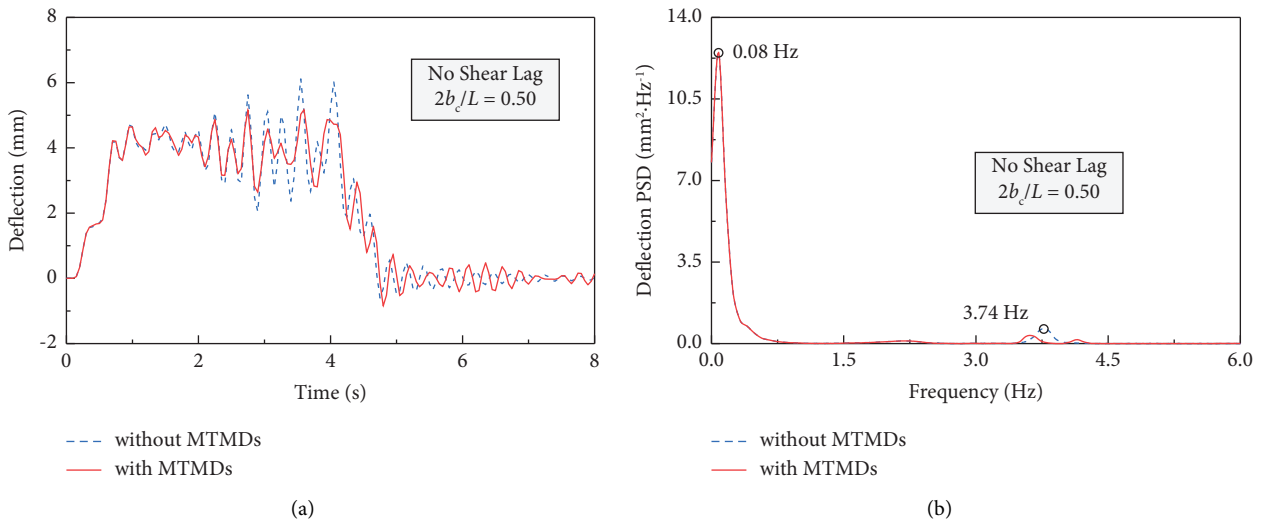

FIGURE 36: Vertical deflection of the bridge at its midspan when $2b_c/L = 0.50$ without shear lag: (a) time history; (b) spectral power density.

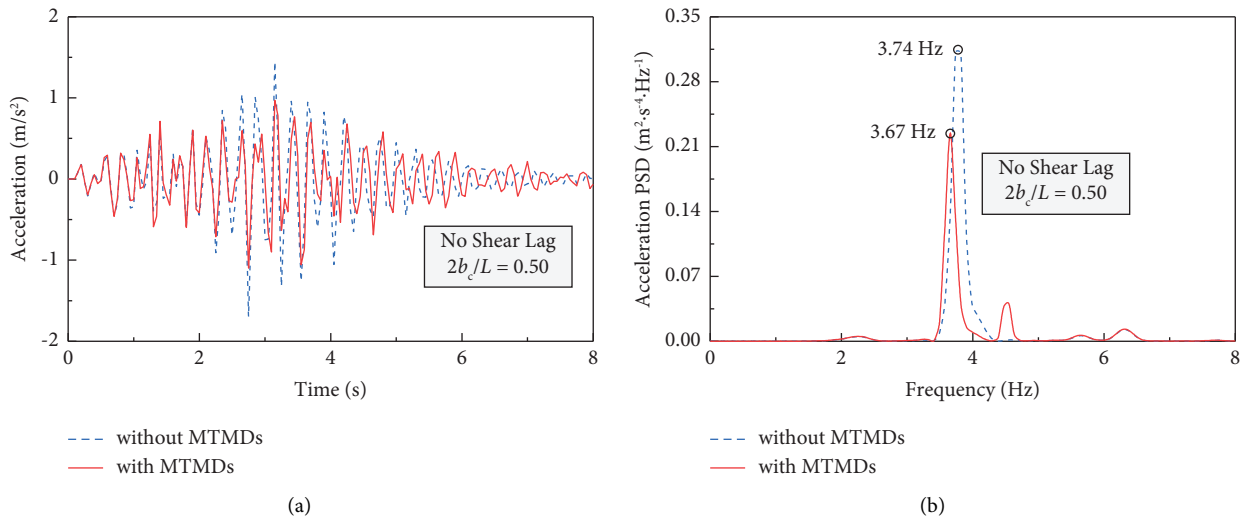

FIGURE 37: Vertical acceleration of the bridge at its midspan when $2b_c/L = 0.50$ without shear lag: (a) time history; (b) spectral power density.

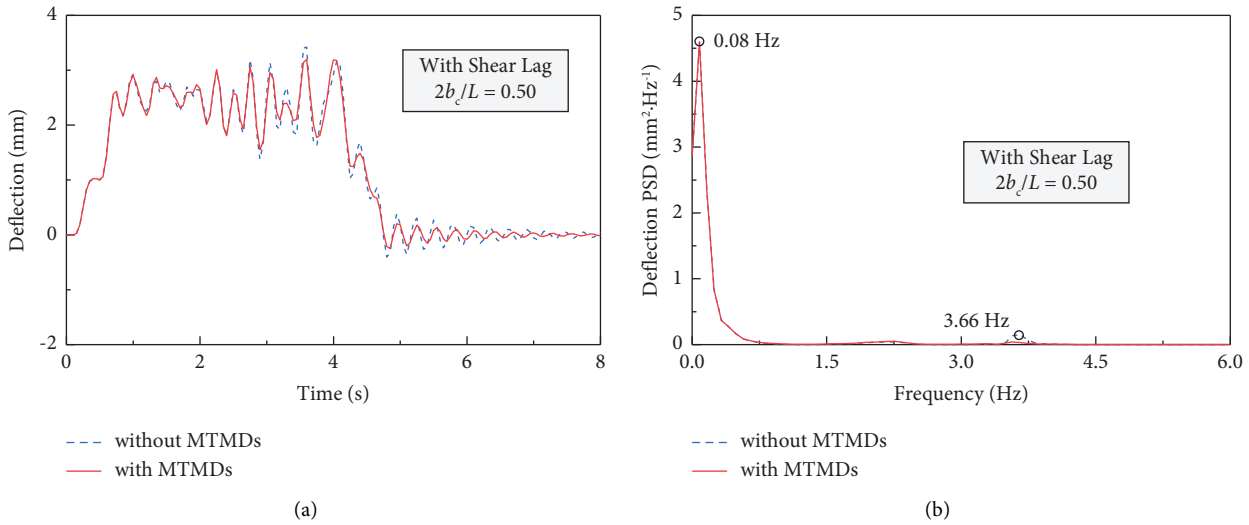

FIGURE 38: Vertical deflection of the bridge at its midspan when $2b_c/L = 0.50$ with shear lag: (a) time history; (b) spectral power density.

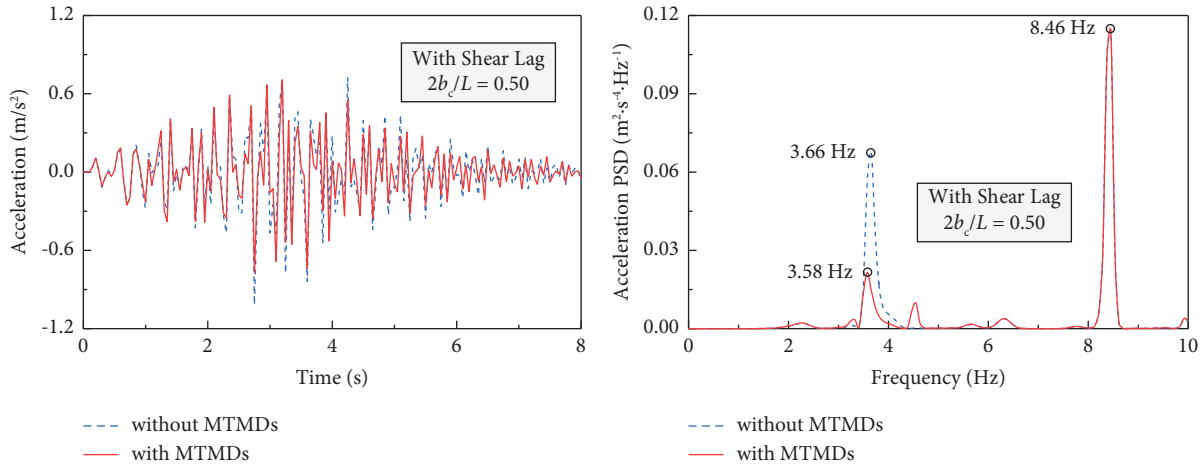

FIGURE 39: Vertical acceleration of the bridge at its midspan when $2b_c/L = 0.50$ with shear lag: (a) time history; (b) spectral power density.

5.4. Shear Lag. As illustrated above, the parameters of trains remained consistent with those in Section 4.1, and the shear connection stiffness ρ_{sh} is 10 kN/m^2, while width-span ratios of the bridge varied, i.e., $2b_c/L = 0.25$ and $2b_c/L = 0.5$.

In this case, the maximum acceleration and deflection of the bridge at its midspan were considered the optimization objective functions. After the optimization by PSM, Tables 5 and 6 specifically show the optimum tuning frequency ratio β_{ti} and damping ratio ξ_{ti} of MTMDs and the maximum dynamic responses of the bridge at its midspan $\ddot{v}_{bl,\max}$ and $v_{bl,\max}$, comparing the results with a shear-lag effect with those without. The vertical acceleration and deflection in both the time history and frequency domains are displayed in Figures 32–39.

Thus, it is clear from above that there is some difference between these two conditions. When $2b_c/L = 0.25$, shear lag of the bridge appears not as pronounced, so the vertical maximum acceleration of the bridge at its midspan increases slightly, and the vertical maximum deflection decreases from 6.109 mm to 6.086 mm, which has little difference because shear lag does not reduce the stiffness of the bridge too much. Thus, the vibration damping ratio of MTMDs for vertical acceleration decreases from 35.12% to 33.39% and that for vertical deflection decreases from 15.65% to 15.63%. However, the MTMD system still plays a role in vibration control. When $2b_c/L = 0.5$, shear lag appears more serious, and the stiffness of the bridge decreases more, which made the vertical maximum acceleration of the bridge at its midspan increase from 0.9625 m/s^2 to 1.0167 m/s^2, and the vertical maximum deflection from 2.806 mm to 3.189 mm but not drastically. However, because shear lag greatly changes the dynamic characteristics of the bridge, the components in the vertical deflection of the bridge increase, and even the peak does not correspond to the fundamental

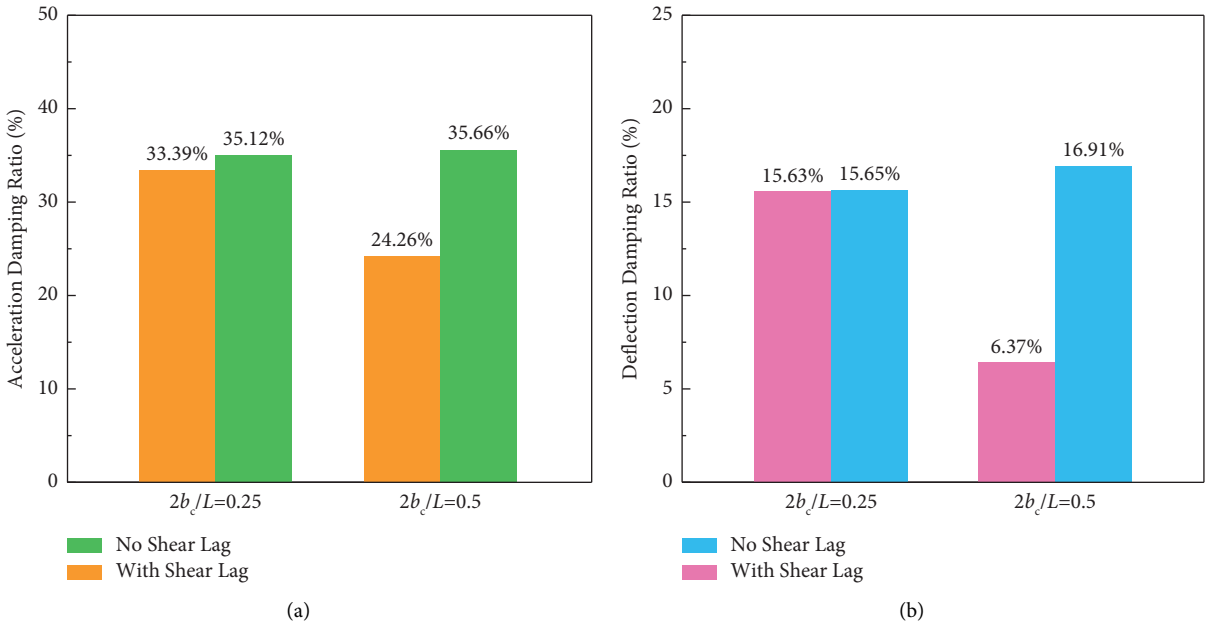

Figure 40: Damping ratios of different width-span ratios.

frequency. To be specific, the vibration damping ratio of MTMDs for vertical acceleration decreases from 35.66% to 24.26% and that for vertical deflection decreases from 16.91% to 6.37%, suggesting that the detuning effect is pronounced and even MTMDs could not control the vibration of the bridge, especially for vertical deflection.

Figure 40 shows a comparison of the vibration damping ratios in the time history between the bridges with and without shear lag. For the vertical acceleration of the bridge at its mid-span, the larger the width-span ratio $2b_c/L$, the greater impact shear lag has on the vibration-damping effect. When the width-span ratio $2b_c/L$ changes from 0.25 to 0.5, the vibration damping ratio considering shear lag of the bridge simply decreases from 33.39% to 24.26%. However, the results are worse for vertical deflection, which drops rapidly from 15.63% to 6.37%.

Therefore, as $2b_c/L$ increases, shear lag affects the distribution of components of the dynamic responses in the frequency domain. This would be aggravated with an increase in $2b_c/L$, and the vibration damping ratio for vertical deflection is seriously weakened. Moreover, in practice, shear lag of the composite girder bridge should be fully taken into consideration of vibration control using MTMDs.

6. Conclusions

In this study, the dynamic analysis model of a complex train-composite box girder bridge-MTMD coupling system is proposed with the derived dynamic equations for the following research. Through the numerical simulation, conclusions can be drawn as follows:

(1) In terms of the strongly coupled and time-varying system, PSM and PSO are better than GA in searching for the optimum parameters to suppress the vibration caused by train-bridge interaction. But the optimization time of PSM is reduced to the minimum, taking advantage of the closed-form Den Hartog's expressions.

(2) The vibration damping ratio for vertical dynamic responses of the bridge increases as the train's number is larger since resonance becomes more obvious, whereas the dynamic characteristics of the bridge do not change in nature.

(3) The vibration damping ratio for vertical dynamic responses of the bridge increases as ρ_{sh} is larger. Meanwhile, the larger the shear connection stiffness, the smaller the increase. However, the decreased shear connection stiffness slightly changes the dynamic characteristics of the bridge and reduces the vibration-damping effect of MTMDs.

(4) When $2b_c/L$ is small, shear lag of the bridge is not pronounced. So the vibration-damping effect of MTMDs slightly decreases, but the device still plays a role. When $2b_c/L$ is large, shear lag of the bridge becomes obvious, decreases the bridge's stiffness, and greatly changes its dynamic characteristics, even the peak of the dynamic response in the frequency domain does not correspond to the fundamental frequency.

(5) Under the train-bridge interaction, both slip and shear lag have a significant influence on the vibration-damping effect of MTMDs. Hence, more attention should be given during every structural stage, such as design, construction, and operation to minimize its hazards.

Appendix

The results of the submatrices of stiffness $\mathbf{K_{tt}}$, mass $\mathbf{M_{tt}}$, and damping $\mathbf{C_{tt}}$ of the MTMD system are as follows:

$\mathbf{K}_{\mathrm{tt}} = \begin{bmatrix} k_{\mathrm{t1}} & & & \\ & k_{\mathrm{t2}} & & \\ & & \ddots & \\ & & & k_{\mathrm{tn}} \end{bmatrix}_{n\times n}$, $\mathrm{M}_{tt} = \begin{bmatrix} m_{\mathrm{t1}} & & & \\ & m_{\mathrm{t2}} & & \\ & & \ddots & \\ & & & m_{\mathrm{tn}} \end{bmatrix}_{n\times n}$, and $\mathbf{C}_{\mathrm{tt}} = \begin{bmatrix} c_{\mathrm{t1}} & & & \\ & c_{\mathrm{t2}} & & \\ & & \ddots & \\ & & & c_{\mathrm{tn}} \end{bmatrix}_{n\times n}$ where n is the total number of TMDs.

The nonzero elements of the stiffness submatrix and damping submatrix in the composite box girder bridge-MTMD coupling system are as follows:

for $i = 1: n$

$\mathbf{K_{bt}}(i, n_{\mathrm{bl}}) = \mathbf{K_{bt}}(i, n_{\mathrm{bl}}) - \mathrm{k_t(i)};$

$\mathbf{K}^{t}_{\mathrm{bb}}(n_{\mathrm{bl}}, n_{\mathrm{bl}}) = \mathbf{K}^{t}_{\mathrm{bb}}(n_{\mathrm{bl}}, n_{\mathrm{bl}}) + k_t(i);$

$\mathbf{C_{bt}}(i, n_{\mathrm{bl}}) = \mathbf{C_{bt}}(i, n_{\mathrm{bl}}) - \mathrm{c_t(i)};$

$\mathbf{C}^{t}_{\mathrm{bb}}(n_{\mathrm{bl}}, n_{\mathrm{bl}}) = \mathbf{C}^{t}_{\mathrm{bb}}(n_{\mathrm{bl}}, n_{\mathrm{bl}}) + c_t(i);$

end

$\mathbf{K_{tb}} = \mathbf{K}^{T}_{\mathrm{bt}}$

$\mathbf{C_{tb}} = \mathbf{C}^{T}_{\mathrm{bt}}$

where $k_t(i) = k_{\mathrm{ti}}$, $c_t(i) = c_{\mathrm{ti}}$, n_{bl} is the n_{bl}-th degree of freedom of the beam element of the composite box girder bridge where the ith TMD is installed, superscript $^{\mathbf{T}}$ represents the transpose of a matrix, and subscript $_{\mathbf{bt}}$ represents the elements of the composite box girder coupled with installed MTMDs.

Data Availability

The data supporting the current study are available from the corresponding author upon reasonable request.

Conflicts of Interest

The authors declare that they have no conflicts of interest.

Acknowledgments

The authors gratefully acknowledge the financial support provided by the Project of Central Guidance for Local Science and Technology Development of China (226Z0801G).

References

[1] M. K. Song, H. C. Noh, and C. K. Choi, "A new three-dimensional finite element analysis model of high-speed train–bridge interactions," *Engineering Structures*, vol. 25, no. 13, pp. 1611–1626, 2003.

[2] D. Huang, "Dynamic and impact behavior of half-through arch bridges," *Journal of Bridge Engineering*, vol. 10, no. 2, pp. 133–141, 2005.

[3] C. H. Lee, M. Kawatani, C. W. Kim, N. Nishimura, and Y. Kobayashi, "Dynamic response of a monorail steel bridge under a moving train," *Journal of Sound and Vibration*, vol. 294, no. 3, pp. 562–579, 2006.

[4] X. Yin, Y. Liu, G. Song, and Y. L. Mo, "Suppression of bridge vibration induced by moving vehicles using pounding tuned mass dampers," *Journal of Bridge Engineering*, vol. 23, no. 7, Article ID 04018047, 2018.

[5] C. D. Stoura and E. G. Dimitrakopoulos, "MDOF extension of the Modified Bridge System method for vehicle–bridge interaction," *Nonlinear Dynamics*, vol. 102, no. 4, pp. 2103–2123, 2020.

[6] Y. Zhang, W. Li, Z. Ji, and G. Wang, "Vehicle ride comfort analysis based on vehicle-bridge coupled vibration," *Shock and Vibration*, vol. 2021, Article ID 5285494, 14 pages, 2021.

[7] C. W. Kim, M. Kawatani, and K. B. Kim, "Three-dimensional dynamic analysis for bridge–vehicle interaction with roadway roughness," *Computers and Structures*, vol. 83, no. 19-20, pp. 1627–1645, 2005.

[8] M. Majka and M. Hartnett, "Effects of speed, load and damping on the dynamic response of railway bridges and vehicles," *Computers and Structures*, vol. 86, no. 6, pp. 556–572, 2008.

[9] Y.-H. Chen and C.-Y. Li, "Dynamic response of elevated high-speed railway," *Journal of Bridge Engineering*, vol. 5, no. 2, pp. 124–130, 2000.

[10] S. H. Ju and H. T. Lin, "Resonance characteristics of high-speed trains passing simply supported bridges," *Journal of Sound and Vibration*, vol. 267, no. 5, pp. 1127–1141, 2003.

[11] H. Nassif and M. Liu, "Analytical modeling of bridge-road-vehicle dynamic interaction system," *Journal of Vibration and Control*, vol. 10, no. 2, pp. 215–241, 2004.

[12] Q. Li, Y. L. Xu, D. J. Wu, and Z. W. Chen, "Computer-aided nonlinear vehicle-bridge interaction analysis," *Journal of Vibration and Control*, vol. 16, no. 12, pp. 1791–1816, 2010.

[13] P. Antolín, N. Zhang, J. M. Goicolea, H. Xia, M. Á. Astiz, and J. Oliva, "Consideration of nonlinear wheel–rail contact forces for dynamic vehicle–bridge interaction in high-speed railways," *Journal of Sound and Vibration*, vol. 332, no. 5, pp. 1231–1251, 2013.

[14] M. H. Al-Sherrawi and S. N. Mohammed, "Shear lag in composite steel concrete beams," in *Proceedings of the 2018 1st International Scientific Conference of Engineering Sciences-3rd Scientific Conference of Engineering Science (ISCES)*, pp. 169–174, Diyala, Iraq, January 2018.

[15] S. He, G. Yang, W. Zhou, Q. Li, and Y. Dong, "Evaluation of shear lag effect in HSS-UHPC composite beams with perfobond strip connectors: experimental and numerical studies," *Journal of Constructional Steel Research*, vol. 194, Article ID 107312, 2022.

[16] C.-S. Wang, W.-T. Zhang, and M.-Y. Yang, "Shear lag effect of composite girders in cable-stayed bridges under dead loads," *Engineering Structures*, vol. 281, Article ID 115752, 2023.

[17] S. Wang, G. Tong, and L. Zhang, "Reduced stiffness of composite beams considering slip and shear deformation of steel," *Journal of Constructional Steel Research*, vol. 131, pp. 19–29, 2017.

[18] J. Sun, Z. Yue, Y. He, and Y. Ibrahim Shah, *Slip Analysis of Prestressed Steel-concrete Continuous Composite Beam*, Journal of King Saud University-Engineering Sciences, Riyadh, Saudi Arabia, 2022.

[19] X. Zheng, W. Li, Q. Huang, and B. Wang, "Finite element modeling of steel-concrete composite beams with different shear connection degrees," *International Journal of Steel Structures*, vol. 21, no. 1, pp. 381–391, 2021.

[20] L. Zhu, R. Kai-Leung Su, and M.-J. Li, "Finite beam element with 26 DOFs for curved composite box girders considering

constrained torsion, distortion, shear lag and biaxial slip," *Engineering Structures*, vol. 232, Article ID 111797, 2021.

[21] H. Wang and E. Zhu, "Dynamic response analysis of monorail steel-concrete composite beam-train interaction system considering slip effect," *Engineering Structures*, vol. 160, pp. 257–269, 2018.

[22] H.-C. Kwon, M.-C. Kim, and I.-W. Lee, "Vibration control of bridges under moving loads," *Computers and Structures*, vol. 66, no. 4, pp. 473–480, 1998.

[23] Y.-H. Chen and Y.-H. Huang, "Timoshenko beam with tuned mass dampers and its design curves," *Journal of Sound and Vibration*, vol. 278, no. 4-5, pp. 873–888, 2004.

[24] X. Shi and C. Cai, "Suppression of vehicle-induced bridge vibration using tuned mass damper," *Journal of Vibration and Control*, vol. 14, no. 7, pp. 1037–1054, 2008.

[25] M. Moghaddas, E. Esmailzadeh, R. Sedaghati, and P. Khosravi, "Vibration control of Timoshenko beam traversed by moving vehicle using optimized tuned mass damper," *Journal of Vibration and Control*, vol. 18, no. 6, pp. 757–773, 2012.

[26] S. Krenk and J. Høgsberg, "Tuned mass absorber on a flexible structure," *Journal of Sound and Vibration*, vol. 333, no. 6, pp. 1577–1595, 2014.

[27] S. Chun, Y. Lee, and T.-H. Kim, "H∞ optimization of dynamic vibration absorber variant for vibration control of damped linear systems," *Journal of Sound and Vibration*, vol. 335, pp. 55–65, 2015.

[28] K. Lievens, G. Lombaert, G. De Roeck, and P. Van den Broeck, "Robust design of a TMD for the vibration serviceability of a footbridge," *Engineering Structures*, vol. 123, no. 15, pp. 408–418, 2016.

[29] C. C. Lin, J. F. Wang, and B. L. Chen, "Train-induced vibration control of high-speed railway bridges equipped with multiple tuned mass dampers," *Journal of Bridge Engineering*, vol. 10, no. 4, pp. 398–414, 2005.

[30] N. Poovarodom, S. Kanchanosot, and P. Warnitchai, "Application of non-linear multiple tuned mass dampers to suppress man-induced vibrations of a pedestrian bridge," *Earthquake Engineering and Structural Dynamics*, vol. 32, no. 7, pp. 1117–1131, 2003.

[31] J.-D. Yau and Y.-B. Yang, "A wideband MTMD system for reducing the dynamic response of continuous truss bridges to moving train loads," *Engineering Structures*, vol. 26, no. 12, pp. 1795–1807, 2004.

[32] J. D. Yau and Y. B. Yang, "Vibration reduction for cable-stayed bridges traveled by high-speed trains," *Finite Elements in Analysis and Design*, vol. 40, no. 3, pp. 341–359, 2004.

[33] J. Li, M. Su, and L. Fan, "Vibration control of railway bridges under high-speed trains using multiple tuned mass dampers," *Journal of Bridge Engineering*, vol. 10, no. 3, pp. 312–320, 2005.

[34] M. Luu, V. Zabel, and C. Könke, "An optimization method of multi-resonant response of high-speed train bridges using TMDs," *Finite Elements in Analysis and Design*, vol. 53, pp. 13–23, 2012.

[35] L. F. F. Miguel, R. H. Lopez, A. J. Torii, L. F. F. Miguel, and A. T. Beck, "Robust design optimization of TMDs in vehicle–bridge coupled vibration problems," *Engineering Structures*, vol. 126, pp. 703–711, 2016.

[36] O. Araz and V. Kahya, "Series tuned mass dampers in vibration control of continuous railway bridges," *Structural Engineering and Mechanics*, vol. 73, no. 2, pp. 133–141, 2021.

[37] F. Gara, G. Leoni, and L. Dezi, "A beam finite element including shear lag effect for the time-dependent analysis of steel–concrete composite decks," *Engineering Structures*, vol. 31, no. 8, pp. 1888–1902, 2009.

[38] L. Zhu, H.-L. Wang, B. Han, G.-Y. Zhao, X.-J. Huo, and X.-Z. Ren, "Dynamic analysis of a coupled steel-concrete composite box girder bridge-train system considering slip and shear-lag," *Thin-Walled Structures*, vol. 157, Article ID 107060, 2020.

[39] J. J. Kalker, *On the Rolling Contact of Two Elastic Bodies in the Presence of Dry Friction*, Delft University of Technology, Delft, Netherlands, 1967.

[40] K. Liu, E. Reynders, G. De Roeck, and G. Lombaert, "Experimental and numerical analysis of a composite bridge for high-speed trains," *Journal of Sound and Vibration*, vol. 320, no. 1-2, pp. 201–220, 2009.

[41] Q.-C. Tang, L. Zhu, and J.-Z. Li, "Hybrid control of steel-concrete composite girder bridges considering the slip and shear-lag effects with MR–TMD based on train-bridge interactions," *Structures*, vol. 47, pp. 2300–2318, 2023.

[42] J. G. Ollgaard, "Shear strength of stud connectors in lightweight and normal weight concrete," *AISC Engineering Journal*, vol. 71, no. 10, 1971.

[43] L. Zhu and R. K. L. Su, "Analytical solutions for composite beams with slip, shear-lag and time-dependent effects," *Engineering Structures*, vol. 152, pp. 559–578, 2017.

[44] L. Wang, S. Z. Liu, S. S. Niu, W. Lu, and A. A. Qin, "Calculation and experimental verification of equivalent damping ratio of new-pattern corrugated steel web composite box girder," in *Proceedings of the 2020 International Conference on Intelligent Transportation Big Data and Smart City (ICITBS)*, pp. 264–268, Vientiane, Laos, January 2020.

[45] L. Frýba, "A rough assessment of railway bridges for high speed trains," *Engineering Structures*, vol. 23, no. 5, pp. 548–556, 2001.

[46] J. P. Den Hartog, *Mechanical Vibrations*, McGraw-Hill, New York, NY, USA, 4th edition, 1956.

[47] G. B. Warburton, "Optimum absorber parameters for various combinations of response and excitation parameters," *Earthquake Engineering and Structural Dynamics*, vol. 10, no. 3, pp. 381–401, 1982.

[48] G. M. Stewart and M. A. Lackner, "The impact of passive tuned mass dampers and wind–wave misalignment on offshore wind turbine loads," *Engineering Structures*, vol. 73, pp. 54–61, 2014.

[49] A. Ghosh and B. Basu, "A closed-form optimal tuning criterion for TMD in damped structures," *Structural Control and Health Monitoring*, vol. 14, no. 4, pp. 681–692, 2007.

[50] Y. Q. Guo and W. Q. Chen, "Dynamic analysis of space structures with multiple tuned mass dampers," *Engineering Structures*, vol. 29, no. 12, pp. 3390–3403, 2007.

[51] B. Fitzgerald and B. Basu, "Cable connected active tuned mass dampers for control of in-plane vibrations of wind turbine blades," *Journal of Sound and Vibration*, vol. 333, no. 23, pp. 5980–6004, 2014.

[52] H. Yamaguchi and N. Harnpornchai, "Fundamental characteristics of Multiple Tuned Mass Dampers for suppressing harmonically forced oscillations," *Earthquake Engineering and Structural Dynamics*, vol. 22, no. 1, pp. 51–62, 1993.